

## A review on shape optimization of hulls and airfoils leveraging Computational Fluid Dynamics Data-Driven Surrogate models

Walker, Jake M.; Coraddu, Andrea; Oneto, Luca

**DOI**

[10.1016/j.oceaneng.2024.119263](https://doi.org/10.1016/j.oceaneng.2024.119263)

**Publication date**

2024

**Document Version**

Final published version

**Published in**

Ocean Engineering

**Citation (APA)**

Walker, J. M., Coraddu, A., & Oneto, L. (2024). A review on shape optimization of hulls and airfoils leveraging Computational Fluid Dynamics Data-Driven Surrogate models. *Ocean Engineering*, 312, Article 119263. <https://doi.org/10.1016/j.oceaneng.2024.119263>

**Important note**

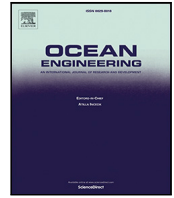
To cite this publication, please use the final published version (if applicable). Please check the document version above.

**Copyright**

Other than for strictly personal use, it is not permitted to download, forward or distribute the text or part of it, without the consent of the author(s) and/or copyright holder(s), unless the work is under an open content license such as Creative Commons.

**Takedown policy**

Please contact us and provide details if you believe this document breaches copyrights. We will remove access to the work immediately and investigate your claim.



# A review on shape optimization of hulls and airfoils leveraging Computational Fluid Dynamics Data-Driven Surrogate models

Jake M. Walker<sup>a</sup>, Andrea Coraddu<sup>a,\*</sup>, Luca Oneto<sup>b</sup>

<sup>a</sup> Delft University of Technology, Delft, Netherlands

<sup>b</sup> University of Genoa, Genoa, Italy

## ARTICLE INFO

### Keywords:

Shape optimization  
Parametrization  
Design of experiments  
Computational Fluid Dynamics  
Data-Driven Models  
Physical plausibility

## ABSTRACT

Shape optimization of vessel hulls and airfoils is crucial for achieving optimal performance and minimizing environmental impact. Typically, these designs are adaptations of existing ones, not fully optimized for specific Key Performance Indicators (KPIs) such as drag or lift, and their optimization often relies on a mix of human experience and numerical approaches. The current state-of-the-art approach leverages Computational Fluid Dynamics (CFD) Data-Driven Surrogate (DDS) models in a four-step process. First, a shape design space is created through parametrization, involving varying levels of human input. Accurate KPI estimation using CFD is computationally intensive, preventing direct optimization. Thus, in the second step, representative shapes are selected from the design space, and evaluated for their KPIs using CFD. Next, a DDS model is constructed from the generated data, which, although costly to develop, allows for efficient KPI prediction. This model is then integrated into an optimization loop to identify optimal geometries on the Pareto front. Finally, these results are validated through CFD to ensure physical plausibility. This review sets focuses on recent advances in DDS models for shape optimization of hulls and airfoils since 2015, an area not thoroughly covered in previous surveys. We systematically examine the four-step optimization process in recent studies, highlighting the evolution and deeper integration of DDS models with CFD. Additionally, we critically assess unresolved issues and gaps in current methodologies, exploring future research directions such as the application of machine learning for shape optimization. These elements highlight the novelty of our work by synthesizing recent technological advances and proposing pathways for future developments, bridging the gap between traditional methods and future possibilities in shape optimization, with implications for both academic research and industrial practice.

## Contents

1.	Introduction .....	2
2.	Problem formalization .....	5
3.	Literature review .....	8
3.1.	Step (1) Shape parametrization, parameter ranges, and KPIs definition .....	8
3.1.1.	Parametrization .....	8
3.1.2.	Ranges .....	10
3.1.3.	KPIs .....	10
3.1.4.	Summary .....	10
3.2.	Step (2) Sampling, data generation, and DDS construction .....	10
3.2.1.	Sampling techniques .....	10
3.2.2.	Data generation with CFD .....	12
3.2.3.	CFD DDS .....	12
3.2.4.	Summary .....	14
3.3.	Step (3) Shape optimization .....	14
3.3.1.	Objectives and constraints .....	14
3.3.2.	Optimizers and performance .....	14

\* Corresponding author.

E-mail addresses: [j.m.walker@tudelft.nl](mailto:j.m.walker@tudelft.nl) (J.M. Walker), [a.coraddu@tudelft.nl](mailto:a.coraddu@tudelft.nl) (A. Coraddu), [luca.oneto@unige.it](mailto:luca.oneto@unige.it) (L. Oneto).

3.3.3. Summary.....	17
3.4. Step (4) Physical plausibility and feedback.....	17
4. Open problems and future perspectives.....	17
5. Conclusion.....	19
CRedit authorship contribution statement.....	20
Declaration of competing interest.....	20
References.....	20

## 1. Introduction

Shape optimization of vessel hulls (Walker et al., 2024; Campana et al., 2006; Tahara et al., 2006; Kostas et al., 2015; Huang and Yang, 2016; Peri, 2016; Cheng et al., 2018; Coppedè et al., 2019; Miao and Wan, 2020; Wang et al., 2020; D'Agostino et al., 2020; Zhang et al., 2021b; Mittendorf and Papanikolaou, 2021; Liu et al., 2022; Wan et al., 2022; Luo et al., 2021; Zhang et al., 2021a) and airfoils (Koziel and Leifsson, 2013; Massaro and Benini, 2015; Zhang et al., 2016; Herrema et al., 2017; Ou et al., 2019; He et al., 2019; Tao and Sun, 2019; Shi et al., 2020; Han et al., 2020; Du et al., 2021; Lye et al., 2021; Raul and Leifsson, 2021; García-Gutiérrez et al., 2022; Shukla et al., 2024; Qu et al., 2017; Hu et al., 2022) describes the new design, or modification of an existing one, to achieve the optimal performance according to the requirements of the specific application. Usually, the optimal hull or airfoil shape is designed to operate with the lowest energy requirements (i.e., efficient fuel usage) and with affordable production processes, driven by economic (Lutz and Wagner, 1998; Nelson et al., 2013; Wang et al., 2015; Ghassemi and Zakerdoost, 2017), environmental (Buckley et al., 2010; Nejat et al., 2014), or a combination of both (Ahmadzadehtalatapeh and Mousavi, 2015) factors. Given the ongoing fluctuations in fuel prices (Yilmaz, 2022; Sala et al., 2022) and the rising efforts to address climate change (Sala et al., 2022), shape optimization of hulls and airfoils is now an important area of research and will continue to remain so for the foreseeable future.

The concept of optimal performance depends on the specific application and is assessed based on one or more Key Performance Indicators (KPIs). KPIs aim to minimize different requirements such as: the energy requirements (consequently, fuel consumption and emissions) (Walker et al., 2024; Campana et al., 2006; Tahara et al., 2006; Kostas et al., 2015; Huang and Yang, 2016; Cheng et al., 2018; Coppedè et al., 2019; Miao and Wan, 2020; Mittendorf and Papanikolaou, 2021; Liu et al., 2022; Koziel and Leifsson, 2013; Zhang et al., 2016; Herrema et al., 2017; Ou et al., 2019; He et al., 2019; Tao and Sun, 2019; Shi et al., 2020; Han et al., 2020; Du et al., 2021; Lye et al., 2021; Raul and Leifsson, 2021; García-Gutiérrez et al., 2022; Shukla et al., 2024; Qu et al., 2017; Wan et al., 2022; Luo et al., 2021; Zhang et al., 2021a; Hu et al., 2022); drag of a hull (Walker et al., 2024; Campana et al., 2006; Tahara et al., 2006; Kostas et al., 2015; Huang and Yang, 2016; Cheng et al., 2018; Coppedè et al., 2019; Miao and Wan, 2020; Wang et al., 2020; Zhang et al., 2021b; Mittendorf and Papanikolaou, 2021; Liu et al., 2022; Wan et al., 2022; Luo et al., 2021; Zhang et al., 2021a); lift and drag of an airfoil (Koziel and Leifsson, 2013; Massaro and Benini, 2015; Zhang et al., 2016; Herrema et al., 2017; Ou et al., 2019; He et al., 2019; Tao and Sun, 2019; Shi et al., 2020; Han et al., 2020; Du et al., 2021; Lye et al., 2021; Raul and Leifsson, 2021; García-Gutiérrez et al., 2022; Qu et al., 2017; Hu et al., 2022); lift and drag of a hydrofoil (Bonfiglio et al., 2018); instability (Gammon, 2011); overheating (Ou et al., 2019); volume (Kenway and Martins, 2016); mass (Tezzele et al., 2023); cost (Kenway and Martins, 2016); or, risk (Júnior et al., 2022).

It is possible to optimize the KPIs of hulls and airfoils in many different ways. Classically, shape optimization involves the adaptation of an existing parent geometry through human experience (Evans, 1959), numerical optimization methods (Reuther et al., 1996; Campana et al., 2006; Tahara et al., 2006; Stück and Rung, 2011), or a mix between

these approaches (Huysse and Lewis, 2001). This, on the one hand, prevents the exploration of non-conventional shapes with possibly better KPIs (Massaro and Benini, 2015; Mittendorf and Papanikolaou, 2021) but, on the other hand, simplifies the manufacturing process being closer to known ones (Albuquerque et al., 2018). Optimizing KPIs is usually based on the evaluation of candidate designs with a virtual experiment using Computational Fluid Dynamics (CFD), which itself varies in both fidelity (Koziel and Leifsson, 2013) and veracity (Stern et al., 2001). However, in recent years, the availability of computational resources and vast amounts of data has opened the door for Data-Driven Methods (Brunton et al., 2020; Vinuesa and Brunton, 2022; Lee and Carlberg, 2020) to gain notoriety in this field of research. In particular, Data-Driven Methods can reduce the computational demand of virtual experiments (Brunton et al., 2020; Kochkov et al., 2021), or replace the need for them all together using a Data-Driven Surrogate (DSS) (Massaro and Benini, 2015; Zhang et al., 2016; Huang and Yang, 2016; Herrema et al., 2017; Bonfiglio et al., 2018; Coppedè et al., 2019; Ou et al., 2019; Tao and Sun, 2019; Miao and Wan, 2020; Shi et al., 2020; Han et al., 2020; Du et al., 2021; Lye et al., 2021; Raul and Leifsson, 2021; Mittendorf and Papanikolaou, 2021; Liu et al., 2022) that is computationally expensive to construct but inexpensive for making predictions that would otherwise require CFD or Experimental Fluid Dynamics (EFD).

The application of the DDS to shape optimization of hulls and airfoils is an area of research that remains vibrant. Previous reviews and surveys on shape optimization methods (Wang and Shan, 2007; Ang et al., 2015; Forrester and Keane, 2009; Kim and Boukouvala, 2020; Leifsson and Koziel, 2016; Koziel and Leifsson, 2016) have primarily focused on the optimization aspects, and, to the best of the authors' knowledge, there is no recent review or survey paper holistically summarizing the state-of-the-art on shape optimization of hulls and airfoils leveraging CFD DDS models. A graphical abstract of this review is reported in Fig. 1.

This review will focus on the four main steps related to shape optimization of hulls and airfoils leveraging CFD DDS models

- Step (1) shape parametrization, parameter ranges, and KPIs definition;
- Step (2) sampling, data generation with CFD possibly integrating already available shapes, and DDS construction;
- Step (3) shape optimization leveraging the CDF DDS;
- Step (4) physical plausibility of the candidate shapes and feedback.

Step (1) deals with the parametrization of the geometry and the definition of the parameter ranges and the desired KPIs for the specific novel hull or airfoil design. The parametrization is responsible for translating the geometry into a numerical representation and must be homomorphic (a unique set of parameters is matched to only one shape in the design space and vice-versa Marinić-Kragić et al., 2016). Parametrization must also be informative (to allow for the prediction of the desired KPIs), intelligible (to allow for interpretation and test the physical plausibility of the results), and synthetic (it must not contain redundant information) (Serani and Diez, 2022). Parameter ranges should be defined based on domain knowledge by domain experts to construct a shape design space large enough to allow for meaningful modifications and small enough to allow for its actual manufacturing (Huang and Yang, 2016; Feng et al., 2018). KPIs should well characterize the performance of the geometry. They can be both explicit (e.g., drag of a hull or lift and drag of an airfoil) or implicit

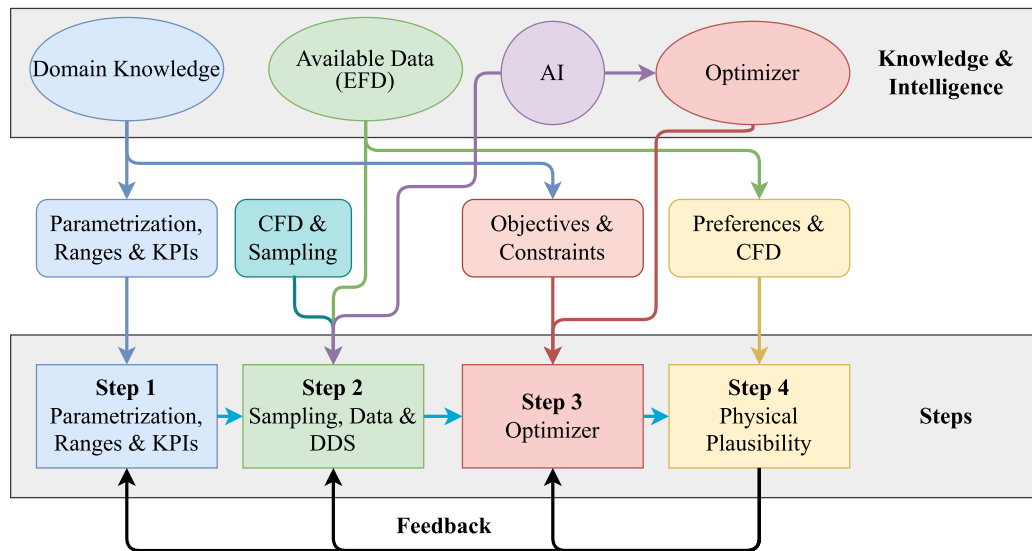


Fig. 1. The graphical abstract of this review.

(e.g., the range of the parameters can impose the fact that some geometries should not be explored since they are too hard to manufacture) (Coppedè et al., 2019; Miao and Wan, 2020; Mittendorf and Papanikolaou, 2021; Liu et al., 2022; Zhang et al., 2016; Herrema et al., 2017; Ou et al., 2019; Tao and Sun, 2019; Shi et al., 2020; Han et al., 2020; Du et al., 2021; Lye et al., 2021; Raul and Leifsson, 2021). Parametrization and parameter ranges affect both the complexity of estimating the KPIs (see Section 3) and the effectiveness of the optimizer in finding designs that can be actually manufactured (Upadhyay et al., 2021). In fact, if we rely solely on CFD to explore a large design space, it is often tricky to calibrate the simulations accurately. If instead, we use a CFD DDS on a large design space, a vast amount of data is necessary that can be hard to retrieve (i.e., relying on EFD data) or computationally expensive to produce (i.e., relying on CFD simulations). For these reasons, Step (1) usually starts with the design requirements, mission profiles, design constraints, and design constraints that define a raw starting point for the design process (Hwang and Martins, 2016; Albuquerque et al., 2018). It is not possible, nor meaningful, to think about a fully automated design process that does not exploit the domain and expert knowledge such as reference geometries and manufacturing constraints (Albuquerque et al., 2018). The level of human intervention in this phase depends on the type of project, its cost, its scope, and delivery time (Cui et al., 2012). Note that these steps deeply influence the quality of final results: a well-constrained design process will facilitate the success of the next steps (Coppedè et al., 2019; Miao and Wan, 2020; Mittendorf and Papanikolaou, 2021; Liu et al., 2022; Zhang et al., 2016; Herrema et al., 2017; Ou et al., 2019; Tao and Sun, 2019; Shi et al., 2020; Han et al., 2020; Du et al., 2021; Lye et al., 2021; Raul and Leifsson, 2021). As we will see later in Section 3.1, a number of approaches to parametrization exist in the literature, either based on modeling shapes in parametric design software (Huang and Yang, 2016; Mittendorf and Papanikolaou, 2021; Liu et al., 2022) or deforming a specific parent shape (Coppedè et al., 2019; Miao and Wan, 2020; Feng et al., 2018; Guerrero et al., 2018; Zhang et al., 2021b; Liu et al., 2022), with both approaches having varying degrees of human intervention and their associated strengths and weaknesses.

Step (2) deals with the accurate estimation of the desired KPIs based on the shape parameters defined at Step (1). In order to perform an accurate estimation, high-fidelity CFD (Duraismy et al., 2019) (e.g., Direct Numerical Simulation if computationally feasible (Shan et al., 2005), or an engineering approximation using Reynolds-averaged Navier–Stokes equations (Massaro and Benini, 2015; Bonfiglio et al., 2018; Ou et al., 2019; Coppedè et al., 2019; Miao and Wan, 2020;

Tao and Sun, 2019; Mittendorf and Papanikolaou, 2021; Raul and Leifsson, 2021; Liu et al., 2022), or Large Eddy Simulation (Barnes and Visbal, 2016)) is needed, but its computational requirements are incompatible with an automated optimization process that usually requires several thousand shapes to be evaluated (Skinner and Zare-Behtash, 2018; Forrester and Keane, 2009; Keane and Voutchkov, 2020) (see Step (3)). In fact, high-fidelity CFD are based on iterative methods to solve the underlying physics of the problem at hand and require a significant computational effort (Wang and Shan, 2007; Leifsson and Koziel, 2016; Harries and Abt, 2019; Keane and Voutchkov, 2020). Low-fidelity CFD are much cheaper in terms of computational requirements (Koziel and Leifsson, 2016), but most of the time much less accurate with respect to high-fidelity CFD (Stern et al., 2001) and still much more computationally demanding with respect to the DDS (Harries and Abt, 2019). In fact, the DDS relies on a simple idea: instead of depending on physical knowledge of the phenomena to make predictions, a model is built based on examples (data) of the input/output (parameters/values or parameters/KPIs) relationships (Kim and Boukouvala, 2020; Jiang et al., 2020) under exam leveraging state-of-the-art Artificial Intelligence (AI), and especially Machine Learning (ML) techniques (Shalev-Shwartz and Ben-David, 2014; Goodfellow et al., 2016; Aggarwal, 2018). The positive aspects of the DDS lie in the fact that the predictions are computationally inexpensive since the function approximating the input/output is cheap to evaluate. For this reason, DDS models have recently attracted the attention of researchers as accurate and computationally inexpensive surrogates of high-fidelity CFD (Coppedè et al., 2019; Miao and Wan, 2020; Mittendorf and Papanikolaou, 2021; Liu et al., 2022; Zhang et al., 2016; Herrema et al., 2017; Ou et al., 2019; Tao and Sun, 2019; Shi et al., 2020; Han et al., 2020; Du et al., 2021; Lye et al., 2021; Raul and Leifsson, 2021). However, this advantage comes with a price. In fact, building a DDS is both data demanding and computationally expensive (Wang and Shan, 2007; Leifsson and Koziel, 2016; Harries and Abt, 2019; Keane and Voutchkov, 2020). For what concerns the data, in-field data requires performing trials (Bai and Wang, 2016; Maniaci et al., 2020) (taking months), EFD data requires model scale tests (Keuning and Katgert, 2008; Huang and Yang, 2016; Feng et al., 2018) (taking weeks), and CFD data requires computationally expensive simulations (Coppedè et al., 2019; Miao and Wan, 2020; Mittendorf and Papanikolaou, 2021; Liu et al., 2022; Zhang et al., 2016; Herrema et al., 2017; Ou et al., 2019; Tao and Sun, 2019; Shi et al., 2020; Han et al., 2020; Du et al., 2021; Lye et al., 2021; Raul and Leifsson, 2021) (taking days). Moreover, building a DDS based on this data requires computationally

intensive procedures, the so-called training phase, which comes with its own computational burden (taking hours) even if this burden is negligible with respect to the one needed to generate or collect the data (Yan et al., 2019). The key advantage of the DDS is that once it is constructed, the forward phase time is negligible (milliseconds or less), enabling its use with any state-of-the-art numerical optimizer (Ruder, 2016; Poli et al., 2007; Vikhar, 2016). For this reason, in Step (2), a few specific and representative shapes are sampled, based on human experience or through more complex strategies (Antony, 2014; Anderson and Whitcomb, 2016), from the design space and fed into the CFD to produce the related data, which is added to possibly already existing data (e.g., in-field or EFD data). This step aims to build a representative dataset of examples to train the DDS (Coppedè et al., 2019; Miao and Wan, 2020; Mittendorf and Papanikolaou, 2021; Liu et al., 2022; Zhang et al., 2016; Herrema et al., 2017; Ou et al., 2019; Tao and Sun, 2019; Shi et al., 2020; Han et al., 2020; Du et al., 2021; Lye et al., 2021; Raul and Leifsson, 2021). The more representative the input/output relation dataset is, the less data is needed for the DDS (Shalev-Shwartz and Ben-David, 2014). Consequently, there are both theoretical and practical reasons to pay appropriate attention at this stage. Theoretically, the database contains the phenomenon we want to learn, and careful consideration regarding the geometry sampling and KPIs estimation is required to capture the desired behavior. Building a representative dataset with a smart sampling strategy is an important and challenging problem per se (Antony, 2014; Anderson and Whitcomb, 2016) and in this survey, we will review the most exploited strategies in the context of hulls and airfoils shape optimization leveraging CFD DDS models (see Section 3.2). Practically, an extensive CFD campaign is often required to build the database, which demands a significant amount of time and computational resources (Coppedè et al., 2019; Miao and Wan, 2020; Mittendorf and Papanikolaou, 2021; Liu et al., 2022; Zhang et al., 2016; Herrema et al., 2017; Ou et al., 2019; Tao and Sun, 2019; Shi et al., 2020; Han et al., 2020; Du et al., 2021; Lye et al., 2021; Raul and Leifsson, 2021). In an ideal world we would rely on already available data (e.g., historical experimental campaigns or simulation) for the dataset to circumvent this challenge. However, at present, this is not always possible due to the lack of historical data and the reliance on very specific parametrizations and parameter ranges that are unique to their particular investigation (Coppedè et al., 2019; Miao and Wan, 2020; Feng et al., 2018; Guerrero et al., 2018; Liu et al., 2022).

In Step (3), we leverage the outputs of Step (1) and Step (2) to automatically search for optimal candidate geometries. For this reason, we are mainly concerned with two connected problems: (i) the formulation of the objective function we want to optimize and (ii) the formulation of the constraints we will apply to the objective. In the context of shape optimization of hulls and airfoils, the objective function is a multi-objective one composed of all the KPIs we want to optimize. Some of these KPIs will be simple functions of the shape geometry parameters (e.g., the volume of a hull), while others can be more complex functions needing a CFD DDS (e.g., the airfoil's drag and lift coefficients). The constraints, instead, are derived from the domain knowledge and represent the fact that not all the parameter space, defined at Step (1), correspond to a feasible shape (e.g., due to cost considerations Wang et al., 2015, performance constraints Coppedè et al., 2019; Miao and Wan, 2020; Mittendorf and Papanikolaou, 2021; Liu et al., 2022; Zhang et al., 2016; Herrema et al., 2017; Ou et al., 2019; Tao and Sun, 2019; Shi et al., 2020; Han et al., 2020; Du et al., 2021; Lye et al., 2021; Raul and Leifsson, 2021, manufacturing constraints International Maritime Organization (IMO), 2022, or regulatory constraints International Maritime Organization (IMO), 2023).

It is worth mentioning that formulating the constraints may also require the computation of complex quantities via a CFD DDS. To deal with the multi-objective nature of the problem, the most common approach is to replace the multiple objectives with a weighted sum of the different objectives (Emmerich and Deutz, 2018) but also other approaches exist (Deb, 2001; Emmerich and Deutz, 2018; Wang and

Shan, 2007; Forrester and Keane, 2009; Ang et al., 2015; Leifsson and Koziel, 2016; Koziel and Leifsson, 2016; Vu et al., 2017; Kim and Boukouvala, 2020; Jiang et al., 2020; Burachik et al., 2022). In this way, the problem becomes a constrained single-objective optimization problem that can be solved with state-of-the-art optimizer (McCall, 2005; Poli et al., 2007; Vikhar, 2016; Ruder, 2016; Kochenderfer and Wheeler, 2022; Swarnkar and Swarnkar, 2020; Burachik et al., 2022). Note that, nowadays, optimizers can also be empowered with AI-based techniques (Swarnkar and Swarnkar, 2020), which allows them to reduce their computational requirements or improve their effectiveness in finding good solutions. Nevertheless, given the multi-objective nature of the original problem, it is required to create the so-called Pareto frontier allowing to find the set of all Pareto efficient solutions (Emmerich and Deutz, 2018; Burachik et al., 2022), namely all the solutions for which is not possible to find more than one objective better than the one of the solutions itself. To tackle this problem, usually, multiple single-objective optimization problems need to be solved (e.g. single-objective problems resulting from the weighted sum of the different objectives of the original multi-objective problem with different configurations of the weights Emmerich and Deutz, 2018) resulting in additional computational overhead (Coppedè et al., 2019; Miao and Wan, 2020; Mittendorf and Papanikolaou, 2021; Liu et al., 2022; Zhang et al., 2016; Herrema et al., 2017; Ou et al., 2019; Tao and Sun, 2019; Shi et al., 2020; Han et al., 2020; Du et al., 2021; Lye et al., 2021; Raul and Leifsson, 2021).

The last step, the Step (4), is probably the most important one not just because it takes the output of all the previous steps to produce a candidate shape but because it also provides feedback and refinements for previous steps able to empower them (Koziel and Leifsson, 2016; Forrester and Keane, 2009). In fact, by exploiting shape design preferences from experienced designers' expertise, it is possible to choose some candidate shapes on the Pareto front, potentially exhibiting the best trade-off between the KPIs for the specific application. This choice obviously does not conclude the design process. In fact, these new shape designs (i) must be physically plausible (e.g., it is actually possible to manufacture them and it is cost-effective) and (ii) must actually provide the required performance. This can be verified with different levels of accuracy (Koziel and Leifsson, 2013; Huang and Yang, 2016; Feng et al., 2018). In the first level, high-fidelity CFD are used since they can surely be exploited to study a few candidate shapes (Coppedè et al., 2019; Miao and Wan, 2020; Mittendorf and Papanikolaou, 2021; Liu et al., 2022; Zhang et al., 2016; Herrema et al., 2017; Ou et al., 2019; Tao and Sun, 2019; Shi et al., 2020; Han et al., 2020; Du et al., 2021; Lye et al., 2021; Raul and Leifsson, 2021). Then a model scale test can be performed to confirm the CFD (Huang and Yang, 2016; Feng et al., 2018). Finally, a field trial will be performed to confirm the results of model scale and CFD results (Min and Kang, 2010; Strasser et al., 2015). If, during this verification, inconsistencies are encountered, or the candidate shape does not exhibit satisfactory performances, these results are used as feedback to modify and improve the previous steps (e.g., modifying the parameter ranges in Step (1), improving the DDS accuracy by including more data in Step (2), or improving the definition of the constraints in Step (3)). Then, the procedure is repeated until a satisfactory design is obtained (Koziel and Leifsson, 2016; Forrester and Keane, 2009).

In this review, it is not possible to consider all the publications in this vibrant field of research due to the large volume of works. Hence, we defined a criteria, taking inspiration from Snyder (2019), to narrow down the top publications according to

- problem category: we focus primarily on shape optimization of hulls and airfoils but, at times, may also include some adjacent shapes;
- publication date: we focus on works published after the year 2015;
- publication quartile: we favor publications in the first quartile (and in some specific cases also the second one) of journals;

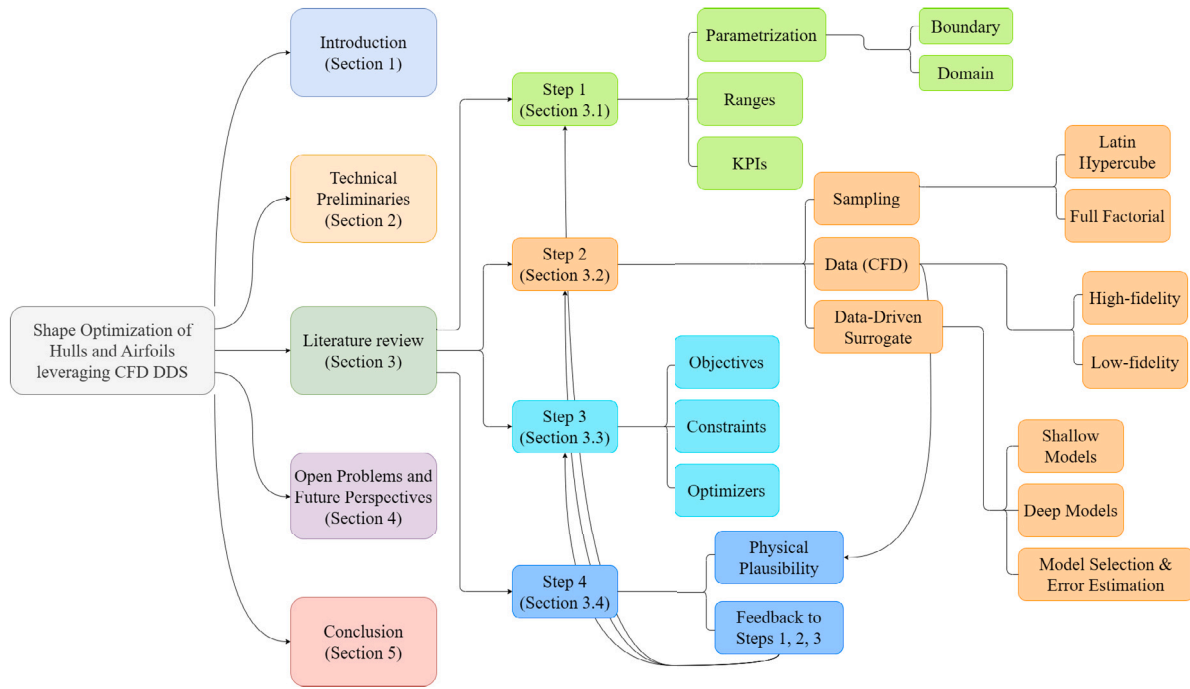


Fig. 2. Graphical table of contents.

- number of citations: we favor journals that have averaged at least three or more citations per year since publication.

Subsequently, we performed a critical review of the narrowed literature accompanied by informative summary tables.

The rest of the review is organized as follows (see Fig. 2). Section 2 contains the problem formalization which is necessary to understand the survey. Section 3 presents the analytical review on shape optimization of hulls and airfoils leveraging CFD DDS models following the four-step approach of Fig. 1. Section 4 discusses the open problems and future perspectives of this vibrant field of research. Finally, Section 5 concludes the review.

## 2. Problem formalization

The goal of shape optimization of hulls and airfoils is to find the optimal shape  $\Omega^*$  in a set of possible ones  $D$ , where  $D$  are all the possible candidate geometries that we can explore given, e.g., cost constraints, performance constraints, manufacturing constraints, or regulatory constraints. The optimality principle is guided by one or more KPIs depending on the specific application, e.g., the drag of a hull (Campana et al., 2006; Tahara et al., 2006; Kostas et al., 2015; Huang and Yang, 2016; Cheng et al., 2018; Coppedè et al., 2019; Miao and Wan, 2020; Wang et al., 2020; D’Agostino et al., 2020; Zhang et al., 2021b; Mittendorf and Papanikolaou, 2021; Liu et al., 2022) or the lift and drag of an airfoil (Koziel and Leifsson, 2013; Massaro and Benini, 2015; Zhang et al., 2016; Herrema et al., 2017; Ou et al., 2019; He et al., 2019; Tao and Sun, 2019; Shi et al., 2020; Han et al., 2020; Du et al., 2021; Lye et al., 2021; Raul and Leifsson, 2021; García-Gutiérrez et al., 2022). We then define, in Step (1),  $k$  KPIs as functions of a particular shape as follows

$$J_i(\Omega) : D \rightarrow \mathbb{R}, i \in \{1, \dots, k\}, \Omega \in D, \quad (1)$$

and consequently, our final goal to optimize shape of hulls or airfoils, can be formalized as follows

$$\min_{\Omega \in D} J_1(\Omega), \dots, J_k(\Omega). \quad (2)$$

Note that,  $\Omega$  is the actual 3D (or in some cases 2D) geometry, which, although technically possible (Kara and Shimada, 2006), is hard to

handle/modify directly through human intervention because there is a vast amount of possible modifications that can be made and it is preferable to structure the modifications with a method that is logical, consistent, and repeatable (Coppedè et al., 2019; Miao and Wan, 2020; Mittendorf and Papanikolaou, 2021; Liu et al., 2022; Zhang et al., 2016; Herrema et al., 2017; Ou et al., 2019; Tao and Sun, 2019; Shi et al., 2020; Han et al., 2020; Du et al., 2021; Lye et al., 2021; Raul and Leifsson, 2021).

For this reason, in Step (1) a particular parent shape  $\Omega^p$  is taken as reference geometry and then  $\Omega \in D$  are parametrized so that a modification vector  $x \in \mathbb{R}^d$  can be applied to  $\Omega^p$  according to a rule  $R$  to generate  $\Omega \in D$  (Massaro and Benini, 2015; Zhang et al., 2016; Huang and Yang, 2016; Herrema et al., 2017; Bonfiglio et al., 2018; Coppedè et al., 2019; Ou et al., 2019; Tao and Sun, 2019; Shi et al., 2020; Han et al., 2020; Du et al., 2021; Lye et al., 2021; Raul and Leifsson, 2021; Liu et al., 2022). Note that this leads to an approximation since

- $R$  may not be able to generate all  $\Omega \in D$  with  $x \in \mathbb{R}^d$  (Massaro and Benini, 2015; Huang and Yang, 2016; Coppedè et al., 2019; Mittendorf and Papanikolaou, 2021);
- some  $x \in \mathbb{R}^d$  applied to the rule  $R$  may generate  $\Omega \notin D$  (D’Agostino et al., 2020; Massaro and Benini, 2015; Zhang et al., 2016; Huang and Yang, 2016; Herrema et al., 2017; Bonfiglio et al., 2018; Coppedè et al., 2019; Ou et al., 2019; Tao and Sun, 2019; Shi et al., 2020; Han et al., 2020; Du et al., 2021; Lye et al., 2021; Raul and Leifsson, 2021; Liu et al., 2022).

For the first problem, the trade-off between exploring more  $\Omega \in D$  and increasing the dimensionality of the parametrization, namely  $d$ , is determined by domain experts (Massaro and Benini, 2015; Huang and Yang, 2016; Coppedè et al., 2019; Mittendorf and Papanikolaou, 2021). For the second problem, some specific  $x \in \mathbb{R}^d$  may lead to  $\Omega \notin D$  (D’Agostino et al., 2020), so we always have to check for this consistency by adding constraints to  $x \in \mathbb{R}^d$  (Massaro and Benini, 2015; Zhang et al., 2016; Huang and Yang, 2016; Herrema et al., 2017; Bonfiglio et al., 2018; Coppedè et al., 2019; Ou et al., 2019; Tao and Sun, 2019; Shi et al., 2020; Han et al., 2020; Du et al., 2021; Lye et al., 2021; Raul and Leifsson, 2021; Liu et al., 2022).

The modification vector  $x$  handles the modifications to  $\Omega^p$  easily, retrieving a particular  $\Omega \in D$ . So  $x$  is just instrumental. The elements in  $x$  must be independent because we must be able to change

every element independently from the others, i.e., two dependent elements would result in a  $(d - 1)$ -dimensional modification vector. In order to define  $R$ , a number of approaches exist in the literature, the two most common being boundary (Gain and Bechmann, 2008) and domain-based parametrizations (Sederberg and Parry, 1986). For the former, in its most naive form,  $R : D \times \mathbb{R}^d \rightarrow D$  can correspond to the displacement of coordinates on the surface of the shape. Whereas, a domain-based parametrization considers a control volume around the shape and the rule corresponds to the displacement of control points for a deformation-based, e.g., a Free-Form Deformation (FFD) parametrization (Sederberg and Parry, 1986). However, regardless of the implementation, the rule  $\Omega = R(\Omega^p, x)$  must be homomorphic (Wang et al., 2022a) and maps a parent shape  $\Omega^p \in D$  into another one  $\Omega \in D$  based on  $x \in \mathbb{R}^d$ . For what concerns the homomorphism of  $R$ , what we require is a bijective homomorphism, namely

$$\exists R^{-1} : R^{-1}(R(\Omega, x), x) = \Omega, \forall x \in \mathbb{R}^d, \Omega \in D, \quad (3)$$

or, in other words, a particular  $x \in \mathbb{R}^d$  corresponds to one and only one modification of  $\Omega \in D$  and vice-versa. Consequently, Problem (2) can be reformulated subject to (s.t.) the described constraints as follows

$$\begin{aligned} \min_{x \in \mathbb{R}^d} \quad & J_1(\Omega), \dots, J_k(\Omega), \\ \text{s.t.} \quad & \Omega = R(\Omega^p, x), \Omega \in D. \end{aligned} \quad (4)$$

Problem (4) remains mathematically and numerically challenging due to the complex relationships between the 3D (or 2D) geometries and the specific KPIs of interest (Koziel and Leifsson, 2016; Forrester and Keane, 2009). For this reason, in Step (1), we need to make some further reformulations and approximations to the problem at hand. For the multi-objectives of Problem (4), namely  $J_i(\Omega)$  with  $i \in \{1, \dots, k\}$ , researchers formulate with different approaches (e.g., High/Low-fidelity CFD (Koziel and Leifsson, 2013)) a more or less accurate estimation of  $J_i^R(x)$  given  $x$  (which varies during optimization) and  $R$  (which is fixed) (Massaro and Benini, 2015; Zhang et al., 2016; Huang and Yang, 2016; Herrema et al., 2017; Bonfiglio et al., 2018; Coppedè et al., 2019; Ou et al., 2019; Tao and Sun, 2019; Miao and Wan, 2020; Shi et al., 2020; Han et al., 2020; Du et al., 2021; Lye et al., 2021; Raul and Leifsson, 2021; Mittendorf and Papanikolaou, 2021; Liu et al., 2022). For the constraints, namely  $\Omega \in D$  with  $\Omega = R(\Omega^p, x)$ , researchers translate them into simple box constraints on  $x$  when possible, i.e.,  $l \leq x \leq u$  where  $l, u \in \mathbb{R}^d$  and  $l \leq u$  (Massaro and Benini, 2015; Ou et al., 2019; Coppedè et al., 2019; Tao and Sun, 2019; Han et al., 2020; Lye et al., 2021; Mittendorf and Papanikolaou, 2021; Raul and Leifsson, 2021; Liu et al., 2022). When this simplification is not possible (e.g., we need to have constraints on physical properties of  $\Omega$ ) researchers translate these constraints into  $c^E$  equality and/or  $c^I$  inequality constraints over more or less accurate functions of  $x$  that approximate the desired properties, namely  $I_i^R(x)$  with  $i \in \{1, \dots, c^I\}$  and  $E_i^R(x)$  with  $i \in \{1, \dots, c^E\}$  (Massaro and Benini, 2015; Huang and Yang, 2016; Bonfiglio et al., 2018; Tao and Sun, 2019; Miao and Wan, 2020; Han et al., 2020; Mittendorf and Papanikolaou, 2021; Raul and Leifsson, 2021). As a consequence Problem (4) is reformulated as follows

$$\begin{aligned} \min_{x \in \mathbb{R}^d} \quad & J_1^R(x), \dots, J_k^R(x), \\ \text{s.t.} \quad & I_i^R(x) \leq 0, i \in \{1, \dots, c^I\}, \\ & E_i^R(x) = 0, i \in \{1, \dots, c^E\}, \\ & l \leq x \leq u. \end{aligned} \quad (5)$$

Problem (5) usually raises computational challenges since, in order to compute some of the  $J_i^R(x)$  with  $i \in \{1, \dots, k\}$ ,  $I_i^R(x)$  with  $i \in \{1, \dots, c^I\}$ , and  $E_i^R(x)$  with  $i \in \{1, \dots, c^E\}$ , the computational requirements may be prohibitive (Harries and Abt, 2019) (e.g., when using High-fidelity CFD Koziel and Leifsson, 2013). In fact, these functions often approximate the physical properties and phenomena of  $\Omega$  and while

in some case an accurate enough estimation can be found with Low-fidelity CFD (Kostas et al., 2015) (which require a comparatively low computational effort), in other cases, High-fidelity CFD are mandatory to reach a desirable level of accuracy (Martineau et al., 2006).

To address this problem, in Step (2), researchers propose to use DDSs. DDSs focus on approximating a complex and computationally expensive function with another function that is computationally expensive to construct but computationally inexpensive to evaluate and is well suited to replace the ones in Problem (5) (Massaro and Benini, 2015; Zhang et al., 2016; Huang and Yang, 2016; Herrema et al., 2017; Bonfiglio et al., 2018; Coppedè et al., 2019; Ou et al., 2019; Tao and Sun, 2019; Miao and Wan, 2020; Shi et al., 2020; Han et al., 2020; Du et al., 2021; Lye et al., 2021; Raul and Leifsson, 2021; Mittendorf and Papanikolaou, 2021; Liu et al., 2022). In particular, given a complex and computationally expensive relation  $\mu : \mathbb{R}^d \rightarrow \mathbb{R}$ , in our case one element in the subset of  $\{J_1^R(x), \dots, J_k^R(x), I_1^R(x), \dots, I_{c^I}^R(x), E_1^R(x), \dots, E_{c^E}^R(x)\}$  that are computationally expensive to evaluate, and a series of  $n$  samples, namely a dataset, of the input-output relation  $S_n = \{(x_1, y_1), \dots, (x_n, y_n)\}$  where  $y_i = \mu(x_i)$  with  $i \in \{1, \dots, n\}$  we are able to generate a model  $f(x)$  which is computationally expensive to build since

- building this model from  $S_n$  using ML is computationally expensive (Ray, 2019);
- retrieving  $S_n$  via CFD or EFD may be hard and is for sure computationally expensive (Campana et al., 2006; Vinuesa and Brunton, 2022). In fact, EFD suitable for the particular design may not be available due to its prohibitive cost (Pena and Huang, 2021; Casalone et al., 2020). If instead we generate data via CFD, sampling a representative set of geometries is already a challenge per se, and then evaluating the performance of each geometry may take months due to the computational complexity of the CFD simulations (Casalone et al., 2020);

but computationally inexpensive to estimate since, for the vast majority of ML algorithms, estimating  $f(x)$  takes fractions of milliseconds (Coraddu et al., 2020).

Upon initial observation, one might question the logic behind this approach. In fact, in order to create the DDS we are spending a significant amount of computational power in both creating  $S_n$  with CFD simulations and  $f(x)$  based on  $S_n$ . It is easy to assume that this computational power can instead be used to solve Problem (5) directly, leveraging CFD simulations to estimate the complex relationships. This assumption is incorrect. In fact, when solving Problem (5) even using state-of-the-art optimizers, it is not uncommon to explore hundreds of thousands, if not millions, of values for  $x$  which may take years if we were to rely solely on CFD for the performance estimation (Casalone et al., 2020). Instead, to build the DDS, only a hundreds (maximum thousands) of samples are required for  $S_n$ , needing only a few months of CFD simulations while building  $f(x)$  may only take weeks (Keane and Voutchkov, 2020). Therefore, the computational savings are in order of magnitude thanks to the DDS (Keane and Voutchkov, 2020; Harries and Abt, 2019).

The problem of building a DDS can be then divided into two main sub-problems

- collecting/generating  $S_n$ ;
- building the actual DDS.

Regarding the first sub-problem, collecting/generating  $S_n$ , it is possible to rely on already available EFD of CFD data when possible (Keane and Voutchkov, 2020; Fahrholz and Caprace, 2022), but, in most cases, data needs to be generated from scratch (Massaro and Benini, 2015; Zhang et al., 2016; Huang and Yang, 2016; Herrema et al., 2017; Bonfiglio et al., 2018; Coppedè et al., 2019; Ou et al., 2019; Tao and Sun, 2019; Miao and Wan, 2020; Shi et al., 2020; Han et al., 2020; Du et al., 2021; Lye et al., 2021; Raul and Leifsson, 2021; Mittendorf and Papanikolaou, 2021; Liu et al., 2022). In this case, the main problem is to decide how to sample the space induced by the modification vector

$\mathbf{x}$ , which is already quite a challenge, and for which several proposals have been developed (Antony, 2014; Anderson and Whitcomb, 2016).

Regarding the second sub-problem, building the actual DDS, it can easily be mapped into a now-classical supervised ML problem, particularly an ML regression problem (Massaro and Benini, 2015; Zhang et al., 2016; Huang and Yang, 2016; Herrema et al., 2017; Bonfiglio et al., 2018; Coppedè et al., 2019; Ou et al., 2019; Tao and Sun, 2019; Miao and Wan, 2020; Shi et al., 2020; Han et al., 2020; Du et al., 2021; Lye et al., 2021; Raul and Leifsson, 2021; Mittendorf and Papanikolaou, 2021; Liu et al., 2022). In regression, we have an input space  $\mathcal{X} \subseteq \mathbb{R}^d$  composed of  $d$  features (in our case the modification vector), an output space  $\mathcal{Y} \subseteq \mathbb{R}$  (in our case one of the subsets of  $\{J_1^R(\mathbf{x}), \dots, J_k^R(\mathbf{x}), I_1^R(\mathbf{x}), \dots, I_{c_I}^R(\mathbf{x}), E_1^R(\mathbf{x}), \dots, E_{c_E}^R(\mathbf{x})\}$  that are computationally expensive to evaluate), and a series of  $n$  samples  $S_n$  where  $\mathbf{x}_i \in \mathcal{X}$  and  $y_i \in \mathcal{Y} \forall i \in \{1, \dots, n\}$ . The scope is to learn the input/output relation  $\mu : \mathcal{X} \rightarrow \mathcal{Y}$  based just on  $S_n$ . Generally,  $\mu$  is a probabilistic relation, but in our case, this relation is induced by, e.g., CFD models, so it is deterministic (Coraddu et al., 2023). An ML regression algorithm  $\mathcal{A}$ , characterized by its hyperparameters  $\mathcal{H}$ , selects a model  $f$  inside a set of possible ones  $\mathcal{F}$  based on the available data  $\mathcal{A}_{\mathcal{H}} : S_n \times \mathcal{F} \rightarrow f$ .

Various ML algorithms exist in the literature (Shalev-Shwartz and Ben-David, 2014; Shawe-Taylor and Cristianini, 2004; Breiman, 2001; Goodfellow et al., 2016). However, according to the no-free-lunch theorem (Wolpert, 2002), there is no *a priori* method for determining the best ML algorithm and best hyperparameters for a specific application for a particular problem, and the only option is to empirically test multiple approaches verifying which is actually the best one. This phase is referred to as model selection (Oneto, 2020). Broadly speaking, there are two main families of ML algorithms: shallow and deep models (Goodfellow et al., 2016; Shalev-Shwartz and Ben-David, 2014). For shallow models,  $\mathcal{X}$  is first mapped, by means of a handcrafted feature engineering phase (Chicco et al., 2022) or by means of a more or less elaborated procedure like the kernel trick (Shawe-Taylor and Cristianini, 2004), into a vector  $\phi(X) \in \mathbb{R}^d$ , named representation, able to well represent  $\mathcal{X}$  while discarding the not useful information (Oneto et al., 2015). For deep models,  $\mathcal{X}$  is mapped into a representation  $\phi(X)$ , but not with a fixed procedure, as  $\phi$  is parameterized and learned directly from the data (Cipollini et al., 2019; Liu and Lang, 2019). Shallow models are the top-performing approaches in the case of non-structured (tabular) data while deep models are the top-performing approaches from structured (e.g., graphs and sequences) data.<sup>1</sup> Moreover, deep models usually require significantly more data with respect to the shallow ones to be trained (Liu and Lang, 2019; Horwath et al., 2020).

The error of  $f$  in approximating  $\mu$  is measured by a prescribed metric  $M : \mathcal{F} \rightarrow \mathbb{R}$ . For what concerns the  $M(f)$  many different metrics are available in literature (Acar, 2015; Shao et al., 2017) both quantitative (e.g., the mean absolute error, the mean square error, the root mean square error, the coefficient of determination, and the mean absolute error in percentage to name a few (Acar, 2015)) and qualitative (e.g., scatter plots of the real versus predicted metrics Shao et al., 2017). In order to estimate the performance of the final model according to the desired metrics the error estimation phase needs to be performed (Oneto, 2020).

Finally, in order to give some insights on what the algorithms actually learned from the data it is required to provide some explainability properties of the learned models (Castelvecchi, 2016; Horwath et al., 2020; Dong and Liu, 2018). For shallow models, feature ranking, namely how much the handcrafted features actually contribute to the prediction, is one of the most effective tools (Dong and Liu, 2018). For deep models attention maps represent the state-of-the-art tools for explanations (Hicks et al., 2021; Innat et al., 2023).

At the end of Step (2) we obtain a new set of functions  $\{J_1^R(\mathbf{x}), \dots, J_k^R(\mathbf{x}), I_1^R(\mathbf{x}), \dots, I_{c_I}^R(\mathbf{x}), E_1^R(\mathbf{x}), \dots, E_{c_E}^R(\mathbf{x})\}$  which are the computationally inexpensive counterparts of  $\{J_1^R(\mathbf{x}), \dots, J_k^R(\mathbf{x}), I_1^R(\mathbf{x}), \dots, I_{c_I}^R(\mathbf{x}), E_1^R(\mathbf{x}), \dots, E_{c_E}^R(\mathbf{x})\}$  where, in some cases, we simply use the original function (if computationally inexpensive) or a surrogate (if computationally expensive). The result of this process is a reformulation of Problem (5) into the following one

$$\begin{aligned} \min_{\mathbf{x} \in \mathbb{R}^d} \quad & \bar{J}_1^R(\mathbf{x}), \dots, \bar{J}_k^R(\mathbf{x}), \\ \text{s.t.} \quad & \bar{I}_i^R(\mathbf{x}) \leq 0, i \in \{1, \dots, c_I\}, \\ & \bar{E}_i^R(\mathbf{x}) = 0, i \in \{1, \dots, c_E\}, \\ & l \leq \mathbf{x} \leq u. \end{aligned} \quad (6)$$

Problem (6) is now computationally tractable and many approaches exist to tackle it (Massaro and Benini, 2015; Zhang et al., 2016; Huang and Yang, 2016; Herrema et al., 2017; Bonfiglio et al., 2018; Coppedè et al., 2019; Ou et al., 2019; Tao and Sun, 2019; Miao and Wan, 2020; Shi et al., 2020; Han et al., 2020; Du et al., 2021; Lye et al., 2021; Raul and Leifsson, 2021; Mittendorf and Papanikolaou, 2021; Liu et al., 2022) and Step (3) exactly deals with this problem. The first challenge of Problem (6) is the fact that it is characterized by multiple objectives. To deal with this challenge, multiple approaches exist (Massaro and Benini, 2015; Ou et al., 2019; Tao and Sun, 2019; Mittendorf and Papanikolaou, 2021; Lye et al., 2021; Miao and Wan, 2020; Emmerich and Deutz, 2018). Nonetheless, the vast majority of them reformulate the problem as a single objective problem as follows

$$\begin{aligned} \min_{\mathbf{x} \in \mathbb{R}^d} \quad & \sum_{i=1}^k \lambda_i \bar{J}_i^R(\mathbf{x}) \\ \text{s.t.} \quad & \bar{I}_i^R(\mathbf{x}) \leq 0, i \in \{1, \dots, c_I\}, \\ & \bar{E}_i^R(\mathbf{x}) = 0, i \in \{1, \dots, c_E\}, \\ & l \leq \mathbf{x} \leq u. \end{aligned} \quad (7)$$

where  $\lambda_i \in [0, 1], \forall i \in \{1, \dots, k\}$  are constants such that  $\sum_{i=1}^k \lambda_i = 1$  that weights more or less a particular objective (Emmerich and Deutz, 2018). Varying  $\lambda_i \forall i \in \{1, \dots, k\}$  in Problem (7) it is possible to find all the possible solutions of Problem (6) (Emmerich and Deutz, 2018). Note that, among all of the possible solutions, just some of them are actually meaningful: the ones on the Pareto front (Liu et al., 2021; Massaro and Benini, 2015), obtained via the Skyline operator (Liu et al., 2021), namely, the solutions that are not dominated by any other one according to at least one objective of Problem (6) (Liu et al., 2021; Massaro and Benini, 2015).

Problem (7) is now a computationally tractable single objective constrained optimization problem, namely a standard optimization problem to be addressed (Massaro and Benini, 2015; Zhang et al., 2016; Huang and Yang, 2016; Herrema et al., 2017; Bonfiglio et al., 2018; Coppedè et al., 2019; Ou et al., 2019; Tao and Sun, 2019; Miao and Wan, 2020; Shi et al., 2020; Han et al., 2020; Du et al., 2021; Lye et al., 2021; Raul and Leifsson, 2021; Mittendorf and Papanikolaou, 2021; Liu et al., 2022). In general, Problem (7) is both non-linear and non-linearly constrained (Massaro and Benini, 2015; Huang and Yang, 2016; Bonfiglio et al., 2018; Tao and Sun, 2019; Miao and Wan, 2020; Han et al., 2020; Mittendorf and Papanikolaou, 2021; Raul and Leifsson, 2021). To address Problem (7), many approaches exist (Ruder, 2016; Poli et al., 2007; Vikhar, 2016) but they can be grouped in two main families

- Problem (7) can be relaxed, either globally or in iterative local stages, into a convex formulation. This transformation enables the use of highly efficient algorithms designed specifically for convex optimization. Specifically
  - global convex relaxation reformulates Problem (7) into another problem which tries to approximate it at best with a single convex objective and a series of convex constraints (Bonfiglio et al., 2018; Han et al., 2020; Lye et al., 2021;

<sup>1</sup> Results from the most popular machine learning website, Kaggle (<https://www.kaggle.com/>) show this to be the case when using real-world data.

Raul and Leifsson, 2021). This approach is not always possible since there is an obvious trade-off between accuracy of the approximation of Problem (7) and convexity of the associated resulting optimization problem (Liu and Lu, 2014);

- iterative local convex relaxation means that, starting from a point the domain of Problem (7), the problem is locally approximated with a linear or quadratic or convex objective and with a convex domain (defined by linear or quadratic or convex constraints). Then, the solution of this convex problem is used as a new starting point, and the steps are repeated until convergence to a local minima (Ruder, 2016). To improve the quality, a multiple starting point approach (colloquially, multi-start), is adopted (Raul and Leifsson, 2021);

- Problem (7) is directly addressed with optimizers that can directly handle non-linear and non-linearly constraint optimization problems (Massaro and Benini, 2015; Ou et al., 2019; Coppedè et al., 2019; Mittendorf and Papanikolaou, 2021; Liu et al., 2022). Examples of these algorithms are the evolutionary algorithms (Vikhar, 2016).

Finally, Step (4) focuses on checking the physical plausibility of the solutions on the Pareto front of Problem (7). In particular, it is important that these solutions do not degenerate into a physically implausible one due to the many different approximations that stem from Problem (2) to Problem (7) (i.e., due to parametrization in Step (1), surrogation in Step (2) (Castelvecchi, 2016; D'Amato et al., 2022; Kalikatzarakis et al., 2023; Coraddu et al., 2023), and optimization in Step (3) (Huang and Yang, 2016; Bonfiglio et al., 2018; Ou et al., 2019; Coppedè et al., 2019; Tao and Sun, 2019; Miao and Wan, 2020; Han et al., 2020; Lye et al., 2021; Mittendorf and Papanikolaou, 2021; Raul and Leifsson, 2021; Liu et al., 2022; Koziel and Leifsson, 2013; Huang and Yang, 2016; Feng et al., 2018; Massaro and Benini, 2015)). This check is usually performed in two stages.

The first stage of checks is performed during surrogation in Step (2) (Castelvecchi, 2016; D'Amato et al., 2022; Kalikatzarakis et al., 2023; Coraddu et al., 2023). In fact, surrogating CFD with a DDS may lead to a loss in physical plausibility due to the fact that the DDS can take shortcuts (Castelvecchi, 2016) hidden in the data in order to learn the desired relation (D'Amato et al., 2022; Kalikatzarakis et al., 2023; Coraddu et al., 2023). This is extremely counterproductive when DDSs are exploited in optimization since these shortcuts can trick the optimizers into solutions that are physically implausible (Coraddu et al., 2023). Therefore, it is worthwhile to check the DDS for physical plausibility by means of two approaches

- the first, is to challenge the DDS into solving increasingly complex extrapolation scenarios (Walker et al., 2024; D'Amato et al., 2022; Kalikatzarakis et al., 2023; Coraddu et al., 2023): the DDS is first trained on a subset of data that represent particular physical conditions (e.g., low cruise speed when predicting the hull resistance) and then tested for accuracy in a different physical conditions (e.g., high cruise speed when predicting the hull resistance). A high accuracy in challenging extrapolation scenarios increases the trust in the DDS and checks for hidden shortcuts in the data (Walker et al., 2024; Kalikatzarakis et al., 2023; Coraddu et al., 2023);
- the second one is to inspect the behavior of the DDS through explainability, that tries to open the black box (Geirhos et al., 2020) of the DDS for an expert to check the learned relation (Moradi and Samwald, 2021).

The second stage of checks is performed during optimization in Step (3) (Huang and Yang, 2016; Bonfiglio et al., 2018; Ou et al., 2019; Coppedè et al., 2019; Tao and Sun, 2019; Miao and Wan, 2020; Han et al., 2020; Lye et al., 2021; Mittendorf and Papanikolaou, 2021; Raul and Leifsson, 2021; Liu et al., 2022; Koziel and Leifsson, 2013; Huang and Yang, 2016; Feng et al., 2018; Massaro and Benini, 2015). In particular, given the solution of the Pareto front, they are checked

for physical plausibility and quality by a series of increasingly complex, time consuming, and costly procedures (Koziel and Leifsson, 2013; Huang and Yang, 2016; Feng et al., 2018; Massaro and Benini, 2015; Bonfiglio et al., 2018; Ou et al., 2019; Coppedè et al., 2019; Tao and Sun, 2019; Miao and Wan, 2020; Han et al., 2020; Lye et al., 2021; Mittendorf and Papanikolaou, 2021; Raul and Leifsson, 2021; Liu et al., 2022). The first one is a check by a human expert who searched for implausible or non-manufacturable features of the geometry (Huang and Yang, 2016; Bonfiglio et al., 2018; Ou et al., 2019; Coppedè et al., 2019; Tao and Sun, 2019; Miao and Wan, 2020; Han et al., 2020; Lye et al., 2021; Mittendorf and Papanikolaou, 2021; Raul and Leifsson, 2021; Liu et al., 2022). This step is crucial since it allows both to verify the quality of the pipeline and gives insights to experts on ideas for geometries that can be reused in other projects. Then, once this step is passed, the geometries are verified to have the desired performance via CFD (Huang and Yang, 2016; Bonfiglio et al., 2018; Ou et al., 2019; Coppedè et al., 2019; Tao and Sun, 2019; Miao and Wan, 2020; Han et al., 2020; Lye et al., 2021; Mittendorf and Papanikolaou, 2021; Raul and Leifsson, 2021; Liu et al., 2022). This check actually gives insights on both parametrization in Step (1) (e.g., the ranges were too tight/loose or the parametrization too rough/detailed), surrogation in Step (2) (e.g., some degenerate solution or inaccuracy of the DDS are discovered), and optimization in Step (3) (e.g., some approximations during optimization were too imprecise). If the CFD checks are passed, EFD are checked (Keuning and Katgert, 2008; Huang and Yang, 2016; Feng et al., 2018). If also EFD checks are passed, sea trials are performed (Bai and Wang, 2016; Maniaci et al., 2020). At each one of these checks, significant human intervention is required to discover issues, criticalities, and provide feedback to the previous step for improvements (Koziel and Leifsson, 2013; Huang and Yang, 2016; Feng et al., 2018; Massaro and Benini, 2015; Bonfiglio et al., 2018; Ou et al., 2019; Coppedè et al., 2019; Tao and Sun, 2019; Miao and Wan, 2020; Han et al., 2020; Lye et al., 2021; Mittendorf and Papanikolaou, 2021; Raul and Leifsson, 2021; Liu et al., 2022; Keuning and Katgert, 2008; Bai and Wang, 2016; Maniaci et al., 2020).

### 3. Literature review

This section will report the actual review of the current literature on the four main steps described in Section 2, summarized in the graphical abstract reported in Fig. 1, and structured as depicted in Fig. 2. Specifically, Section 3.1 reviews Step (1), Section 3.2 reviews Step (2), Section 3.3 reviews Step (3), and Section 3.4 reviews Step (4).

#### 3.1. Step (1) Shape parametrization, parameter ranges, and KPIs definition

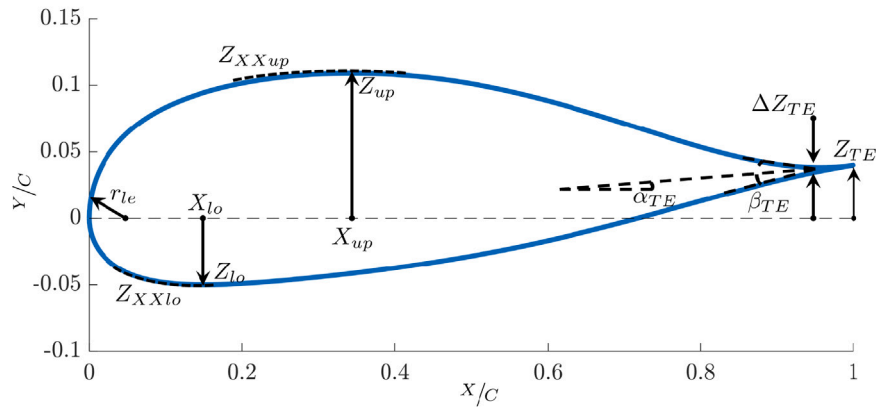
As previously described, Step (1) mainly deals with three aspects: parametrization, parameters ranges, and KPIs definition that will be reviewed in Sections 3.1.1, 3.1.2, and 3.1.3 respectively. Section 3.1.4 will summarize the main work in the literature according to the most critical aspects identified during the review of the three main aspects related to Step (1).

##### 3.1.1. Parametrization

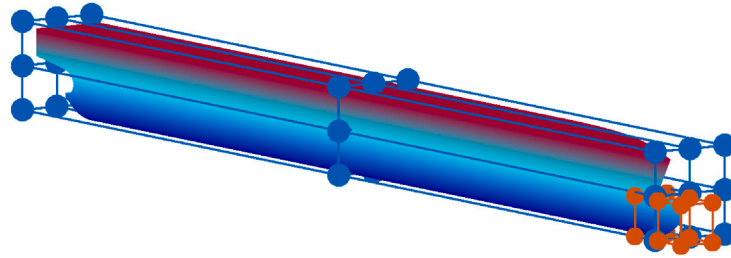
Parametrization deals with translating the modification of a particular parent geometry (e.g., a hull or airfoil) into a numerical representation through a modification vector. The dimensionality of the modification vector, in coordination with the parameter ranges, defines the shape design space.

In general, it is possible to find two dominant approaches to parametrization in the literature

- Boundary-based parametrization: concerns parametrizing the boundary of the shape based on splines or physical attributes (e.g., length, breadth, depth, etc.) to drive the design;



(a) Boundary-based parametric model of an airfoil utilizing the PARSEC-11 parameters [149].



(b) Domain-based (e.g., FFD) parametrization of a hull with both global and local CVs.

Fig. 3. Boundary and domain-based parametrizations.

- Deformation-based parametrization: concerns parametrizing the domain surrounding a parent geometry and uses non-physical descriptors to describe modifications from the parent shape (e.g., Free-Form Deformation).

Both of these approaches are demonstrated in Fig. 3.

**Boundary-based parametrizations.** Boundary-based parametrizations exist in many forms in the literature. Every parametrization is specific to the considered shape.

For airfoils, it is possible to parametrize a geometry with the Class/Shape function Transformation (CST) approach (Kulfan, 2008) demonstrated in Han et al. (2020). Similarly, the Hicks-Henne approach (Masters et al., 2017; Lye et al., 2021) enables the parametrization of an airfoil with 2÷25 design variables. Whereas the PARSEC-11 approach (Sobieczky, 1999) (leveraged in Raul and Leifsson (2021)) describes an airfoil with 11 parameters (shown in Fig. 3(a)) by defining: the leading edge radius ( $r_{le}$ ), the upper and lower curvature ( $Z_{XXup}$  and  $Z_{XXlo}$  respectively), the coordinates of the lowest point on the  $XZ$  plane ( $X_{lo}$ ,  $Z_{lo}$ ), the coordinates of the highest point on the  $XZ$  plane ( $X_{up}$ ,  $Z_{up}$ ), the wedge angle ( $\beta_{TE}$ ), the trailing edge angle ( $\alpha_{TE}$ ), the height of the trailing edge ( $Z_{TE}$ ), and finally, the trailing edge thickness ( $\Delta Z_{TE}$ ).

The most dominant boundary parametrizations for hulls and airfoils are curves or parametric models, or a combination of both. Parametrizations based on curves (Zhang and Zhang, 2015; Luo and Lan, 2017; Wan et al., 2022; Walker et al., 2024), for example, Bezier curves (Derksen and Rogalsky, 2010) and Non-Uniform Rational B-Spline (NURBS) (Shamsuddin et al., 2006; Zhang et al., 2021a), develop a relationship between the design parameters and the feature curves that define the geometry (either through control points or another functional relationship). It is worth mentioning that shape parametrizations based on this approach can lead to high dimensional parameter representations for complex geometries, and while there is a clear benefit to increasing the size of the shape design space, the resulting parametrization requires larger computational efforts with regard to the construction of a dataset and the optimization (see Sections 3.2

and 3.3). For this reason, the number of free parameters following this approach is usually reduced to around 6÷14 in the referenced works, and the performance of the DDS models is between  $\sim 2\div 4\%$  (Zhang and Zhang, 2015; Luo and Lan, 2017; Zhang et al., 2021a). However, preserving physical relevance in the parametrization scheme allows the geometries to be easily reconstructed from their parametric representations and the importance of each parameter remains intuitive (Zhang and Zhang, 2015; Peri, 2016; Luo and Lan, 2017; Luo et al., 2021). Maintaining the physicality of the parameters has a key advantage for reconstructing the geometry and preserving the knowledge obtained through shape optimization. Additionally, when the physical attributes of the model are used in the parametrization, it becomes easier for the human-machine interaction and to interpret the results of the optimization. The referenced works (Huang and Yang, 2016; Moore et al., 2016) include using physical attributes in the parametrization and found performance increases of  $\sim 2\div 9\%$ .

**Domain-based parametrizations.** Domain-based parametrizations (Gain and Bechmann, 2008) involves the definition of Control Volumes (CVs) on the geometry and can be placed on local areas of interest (i.e., the bulbous bow of a vessel hull (Zhang et al., 2017; Guerrero et al., 2018)), globally (i.e., covering the entire geometry), or in multiple parts to investigate a shape design space that covers global and local influences (Miao and Wan, 2020). Fig. 3(b) shows a hull with CVs defined over both global and local regions.

FFD (Sederberg and Parry, 1986) is a popular and effective choice for domain-based parametrizations as demonstrated in a number of studies (Zhang et al., 2017; Guerrero et al., 2018; Zhang et al., 2021b; Demo et al., 2018; Miao and Wan, 2020; Coppedè et al., 2019; Wang et al., 2020; Hu et al., 2022). During this approach, a CV is defined on a parent shape, which is characterized by a number of control points, and the shape modification rule is directly related to the displacement of one or more control points. Often control points will be grouped together in the CV using a simple function (e.g., linear, quadratic) (Demo et al., 2018) to displace a group of control points according to a single parameter. This grouping of control points reduces

both the dimensionality of the parametrization and the likelihood of inducing physically implausible designs.

In general, the referenced works were able to exploit deformation methods to optimize complex shapes based on the specified KPIs, and achieve performance improvements ranging from approximately  $\sim 2\div 12\%$ . However, the key drawback of this approach is the relation between deformation parameters and their physical meaning to the original shape. Consequently, without careful tuning of the parametrization scheme through human intervention, there is a tendency for domain-based parametrizations to induce physically implausible designs which is often dealt with by imposing strict constraints on the design space (i.e., making very small modifications (Huang and Yang, 2016; Miao and Wan, 2020; Hu et al., 2022)) or via constraints based on a physical property of the shape (Huang and Yang, 2016; Miao and Wan, 2020). Furthermore, each parametrization scheme is unique to the parent shape and the specific domain. Consequently, it is not possible to generalize the findings from a deformation-based optimization into physically meaningful information that can be used in other shape optimization tasks.

### 3.1.2. Ranges

The parametrization used in shape optimization must meet several, sometimes conflicting, requirements. For instance, it should be sufficiently informative to predict geometry KPIs, be homomorphic, and avoid containing redundant information. The parameter ranges (in coordination with the parametrization dimensionality) define the shape design space around the parent design that the optimizer can explore to find the best candidate. Making the ranges suitably large is important to ensure an optimal candidate in the shape design space. However, too large ranges combined with too many features in the parametrization can suffer from the curse of dimensionality (Altman and Krzywinski, 2018) and prevent the optimizer from finding the best design in an adequate time.

For what concerns the ranges in the referenced works, exploring airfoil designs in 2-dimensions makes this task simple: as the parameter ranges are bound within the  $XZ$  plane, the design space is bound within the interval  $[0, 1]$  along both axes (i.e.,  $[0, 1] \times [0, 1]$ ) (Tao and Sun, 2019).

For hulls, the ranges are more complex because the shapes are modeled in 3 dimensions instead of 2, and constrained more rigorously to reduce the likelihood of inducing infeasible designs (see Section 3.3). Additionally, because it is easy to induce infeasible designs, the parameters ranges are kept deliberately small in practice. This restricts the admissible space around a known feasible design and reduces the likelihood of the DDS inducing the optimizer into physically implausible candidate shapes.

### 3.1.3. KPIs

In most cases where the shape optimization aimed to minimize the energy requirements, the KPIs were obtained directly from the CFD model (Bonfiglio et al., 2018; Coppedè et al., 2019; Huang and Yang, 2016; Han et al., 2020; Mittendorf and Papanikolaou, 2021) (i.e., lift, drag, or both) or through coefficients derived from the output of the CFD model such as the Coefficients of lift and drag ( $C_L$  and  $C_D$  respectively) (Massaro and Benini, 2015; Ou et al., 2019; Raul and Leifsson, 2021; Lye et al., 2021; Tao and Sun, 2019). Other KPIs were also demonstrated for investigations for priorities outwith minimizing the energy requirements. The heat flux ( $Q$ ) was minimized on the jet thermal protection system (Ou et al., 2019) to improve safety and performance. The stall angle of an airfoil was maximized in Raul and Leifsson (2021) to improve performance. The coefficient of discharge ( $C_{DC}$ ) was optimized for the exhaust nozzle.

It is also worth mentioning that KPIs are often solved for different operating conditions, e.g., velocity (Miao and Wan, 2020), Mach number<sup>2</sup> (Ma) (Tao and Sun, 2019), or Froude Number<sup>3</sup> (Fr) (Huang and Yang, 2016; Coppedè et al., 2019) according to the design requirements of the specific application.

### 3.1.4. Summary

Based on the review performed in Sections 3.1.1, 3.1.2, and 3.1.3 we reported in Table 1 the most important works which deal with Step (1) considering the main different critical and fundamental aspect that raised during the review process

- Parent Geometry: the shape subject that has been optimized;
- Param.: the parametrization method leveraged;
- Param. Dim.: the dimensionality of the parametrization;
- Rule: the implementation of the parametrization;
- Ranges: the size of the shape design space;
- KPIs: the KPIs that that works decided to optimize.

Summarizing Table 1, the critical aspect of Step (1) is to create a suitably large shape design space (in terms of dimensionality of the parametrization and the parameter ranges) so that an optimal design exists while ensuring the relationship between the parameters and KPIs can be easily captured in the ensuing steps. It is worth mentioning that while the shape design space is unique for each of the investigations, it is still meaningful to look at the state-of-the-art approaches to constructing the shape space for each parent geometry. For air/hydrofoils the referenced works usually relied on parametrizations with a dimensionality of  $5\div 17$  (Ou et al., 2019; Bonfiglio et al., 2018), while for hulls there were usually  $5\div 7$  (Coppedè et al., 2019) parameters.

## 3.2. Step (2) Sampling, data generation, and DDS construction

Step (2) deals with three aspects: sampling techniques for the candidate geometries (Section 3.2.1), data generation with CFD (Section 3.2.2), and CFD DDS (Section 3.2.3) for the accurate estimation of the desired KPIs based on the shape parameters defined in Step (1). Section 3.2.4 will summarize the main work in the literature according to the most critical aspects identified during the review of the three main aspects related to Step (2).

### 3.2.1. Sampling techniques

In the referenced works, there are two favored approaches to sampling. The first one is Latin Hypercube Sampling (LHS) (Viana, 2016; Anderson and Whitcomb, 2016) where a multidimensional space is defined either randomly or structured so that the samples are distributed through all of the dimensions. The second one, which is the Full Factorial (FF) Design of Experiments (DoE) (Antony, 2014), involves constructing the full distribution of every possible factorial and then drawing (randomly) from that space. The LHS approach have been previously used in Bonfiglio et al. (2018), Coppedè et al. (2019), Huang and Yang (2016), Han et al. (2020), Miao and Wan (2020), Mittendorf and Papanikolaou (2021) and Raul and Leifsson (2021) and is overwhelmingly the preferred choice to fill vast multidimensional design spaces. It is also worth mentioning that Orthogonal Sampling (OS), which extends the principles of the LHS DoE, is also demonstrated in the literature (Ou et al., 2019). The key difference between LHS and OS lies in the fact that OS specifically aims to uniformly distribute samples across the dimensions of the design space, making it a more structured approach compared to LHS and is reported to require less samples than LHS to well-represent the design space (Ou et al., 2019). On the other hand, the FF DoE approach is also an effective choice (Coraddu

<sup>2</sup> The Mach Number is the ratio between the flow velocity and the speed of sound.

<sup>3</sup> The Froude Number is the ratio between the flow inertia and the gravitational forces, and is proportional to the velocity.

**Table 1**

Most important works which deal with Step (1) considering the shape subject that has been optimized (Parent geometry), the parametrization method leveraged (Param.), the dimensionality of the parametrization (Param. Dim.), the implementation of the parametrization (Rule), the size of the shape design space (Ranges), and the KPIs the work decided to optimize (KPIs).

Ref.	Parent geometry	Param.	Param. Dim.	Rule	Ranges	KPIs
Massaro and Benini (2015)	Airfoil	B-Spline	14	B-spline approach that allows the complete description of an airfoil using control points.	$x/c \in [0, 1]$ $y/c \in [0, 1]$	$C_L$
Huang and Yang (2016)	Hull	FFD/B-spline	5–10	FFD & B-spline functions & 539 Control points governed by 10 parameters	Constraints on bulbous bow (width, height, and angle) and Section area curves of entrance, fore, run, and aft of vessel.	Drag
Bonfiglio et al. (2018)	Hydrofoil	B-Splines	17	4 curves for 2d sections then scaled into 3d	Narrow bounds selected around the original design.	Drag
Ou et al. (2019)	Airfoil (thermal protection system)	Design parameters	5	25 RANS model simulations according to Orthogonal test design method DoE with 4 factors (5 levels per factor) and operating pressure.	$l/d \in [0.5, 1.5]$ $d/d \in [0.0625, 0.3125]$ $PR \in [0.2, 0.6]$ $r_o/d \in [0.016, 0.024]$	$C_D$ & $Q$
Coppedè et al. (2019)	Hull	FFD	7	7 parameters depending on how deformed the sections are [0 – 1] with a design space characterized by $10^7$ possible configurations.	FFD parameters were bound within [–1, 1].	Drag
Tao and Sun (2019)	Airfoil	Design parameters	5	Five-order CST (class/shape function transformation) to govern 39 design parameters.	$x \in [0, 1]$ $y \in [-0.1, 0.2]$	$C_D$ at $Ma = [0.765, 0.775, 0.785, 0.795, 0.805]$
Miao and Wan (2020)	Hull	FFD	5	FFD with 5 parameters functionally linked to groups of control points.	Geometric constrains so maximum variation in displacement or surface area is 1%	Drag at $Fr = [0.2, 0.26]$
Han et al. (2020)	Airfoil	Design parameters	17	2d section of wing plotted in $x/c$ and $y/c$ .	Design space was defined by expanding coefficients by 1.5 times and narrowing by half.	Drag
Lye et al. (2021)	Airfoil	Design parameters	7	C-grid mesh deformed using a thin plate splines based radial basis function interpolation around the airfoil according to Hicks–Henne parameters.	All parameters bound in [0, 1].	$C_L$ & $C_D$
Mittendorf and Papanikolaou (2021)	Hull	Design parameters	6	Parametric model of a catamaran	Designs vary the length and area of the vessel.	Drag
Raul and Leifsson (2021)	Airfoil	PARSEC-11	6	8 Parameters linked to physical attributes and B-Splines.	Parameters bounded to ensure a typical shape is retrieved.	Stall Angle
Liu et al. (2022)	Hull	FFD coupled with splines	5	3 FFD parameters & 2 splines parameters.	Ranges bound within $\pm 15\%$ of ship waterline length.	Drag
Walker et al. (2024)	Hull	B-Spline Curves	32	32 Control points to define the B-Splines of different hull sections.	Ranges bound within margins determined from real vessels.	Drag
Luo et al. (2021)	Hull	Design parameters	5	Maximal radius, Coefficient of minimal radius of the rear body, parallel body length, tail fat index, and tail smoothing index.	Ranges bound within small margin determined by experimental results.	Drag
Wan et al. (2022)	Hull	Design parameters	6	3 parameters for longitudinal, transverse, and length ratio dimensions of hull, and 3 parameters based on fusion factors to apply deformations to the initial cross-section.	Ranges bound within [0, 1].	Drag

(continued on next page)

et al., 2020). The difference between LHS/OS and FF DoE is important because the LHS/OS involves drawing the samples from a distribution which is a subspace of the one we use in the case of FF DoE. In fact, no matter how many samples we draw to form the LHS/OS subspace, this distribution is fixed, whereas we can keep re-sampling from the FF

approach without drawing from a separate distribution. Beyond LHS, OS, and FF DoE, it is worth mentioning that other sampling techniques exist and are demonstrated in the literature. In Liu et al. (2022) authors employ the Sobol sampling method which is a method designed to space out samples more evenly than drawing from a purely random

Table 1 (continued).

Ref.	Parent geometry	Param.	Param. Dim.	Rule	Ranges	KPIs
Hu et al. (2022)	Airfoil	FFD	10	5 FFD parameters on top and bottom sides of airfoil.	Ranges bound within $\pm 10\%$ of airfoil chord length.	Lift to Drag ratio.
Zhang et al. (2021a)	Underwater glider	NURBS	12	Thickness factor and Rotation angle in z-direction for 6 airfoil sections.	Ranges fixed empirically.	Lift to Drag ratio.

distribution. Additionally, in Tao and Sun (2019), authors leverage Gibbs sampling method based on Markov Chain Monte Carlo methods.

Apart from the sampling technique, it is also worth considering the proportion of the design space that is sampled to build the DDS. Obviously, this problem is dependent on the task at hand and depends not only on the dimensionality of the design space but also on the sensitivity of the model to changes in the design parameters (i.e., the complexity of the underlying phenomenon). Therefore, from the referenced works, we can only deduce heuristics in relation to the dimensionality of the problem and the task at hand. The best DDS (i.e., that could approximate the output of the HF model with an error of just a few %) have a ratio  $\rho$  of

$$\rho = \frac{\text{number of samples}}{\text{dimensionality of the parametrization}} \quad (8)$$

of minimum 65 (Bonfiglio et al., 2018) and more typically 300–500 (Mittendorf and Papanikolaou, 2021). Furthermore, in Coppèdè et al. (2019) the authors show the effect of the number of samples on the accuracy of the DDS. They found that when using a  $\rho$  ratio of between 4–8 the accuracy of the DDS was relatively stable. However, the DDS accuracy was significantly improved when the  $\rho$  ratio was increased to 17 which is in line with expectations.

### 3.2.2. Data generation with CFD

Regarding the data needed to develop the DDS we need to leverage CFD to estimate the KPIs defined in Section 3.1.3, for each of the sampled geometries defined in Section 3.2.1, based on their corresponding parameters value defined in Section 3.1.1.

In general, there is a wide degree of fidelity can be obtained from different CFD models. On one hand, Reynolds Averaged Navier Stokes (RANS) (Hirsch, 2007; Andersson et al., 2011) models are usually considered the gold standard High-Fidelity (HF) approach and can also include unsteady/turbulent extensions, but even this method can vary in trustworthiness (Stern et al., 2001) and fidelity (Koziel and Leifsson, 2013). On the other hand, Low-Fidelity (LF) models, e.g., boundary methods (Hall, 1994; Choi et al., 2001), are much less accurate but can still make useful inferences for shape optimization problems.

Aerodynamic modeling using RANS CFD was demonstrated in Han et al. (2020), Massaro and Benini (2015), Ou et al. (2019) and Raul and Leifsson (2021) and an LF approach (Euler methods) in Lye et al. (2021). Hydrodynamic modeling using RANS CFD was demonstrated in Bonfiglio et al. (2018), Coppèdè et al. (2019) and Miao and Wan (2020) and LF models, e.g., Neumann–Michell (NM) (Noblesse et al., 2013) were applied in Miao and Wan (2020) to reduce the computational complexity of an HF CFD model, and Boundary Element Method (BEM) (Hall, 1994; Choi et al., 2001) is also an effective choice of model (Coraddu et al., 2020) if it is accurate enough for the problem at hand. Additionally, a multi-fidelity approach to shape optimization was proposed in Tao and Sun (2019) where the authors used a limited number of HF samples (5) and 19 LF samples to fill the design space.

One of the key concerns for the CFD models regards the validation of the ground truth and, subsequently, the trustworthiness of the data. CFD models are often validated on experimental data (Bonfiglio et al., 2018) which is the preferred method for validating virtual experiments (Stern et al., 2001). Additionally, there are methods for validating mesh convergence during independent studies to improve the reliability and trustworthiness of the CFD (Stern et al., 2001; Martineau et al., 2006).

Regarding the accuracy of CFD models for shape optimization, the referenced works employed various methods depending on the problem at hand. For the resistance prediction or airfoils and hull forms, it is clear that HF RANS models are the favored tool, and the best models out of the referenced works (i.e., those characterized by DDS that could approximate the output of the HF model with a small error 1–5%) typically used the unsteady RANS CFD simulations with turbulence (Bonfiglio et al., 2018; Miao and Wan, 2020; Mittendorf and Papanikolaou, 2021). This is explained by the fact this model determines a more accurate representation of the underlying phenomenon to capture the relationship between shape and performance accurately.

It is also worth mentioning that it is possible to develop the database using both LF and HF data, as was demonstrated in a couple of works (Liu et al., 2022; Han et al., 2020), but some careful consideration is required in this case. Too little HF data leads to an LF dominant DDS characterized by insufficient accuracy for shape optimization. Too much HF data does not allow the LF data to play its part (Liu et al., 2022). Although, if the correct balance between HF and LF is struck the variable fidelity approach can outperform single fidelity (Han et al., 2020). For this reason, and according to the current literature on the topic, single-fidelity sampling is the preferred approach for DDS-based shape optimization (Massaro and Benini, 2015; Huang and Yang, 2016; Bonfiglio et al., 2018; Ou et al., 2019; Coppèdè et al., 2019; Miao and Wan, 2020; Lye et al., 2021; Mittendorf and Papanikolaou, 2021; Raul and Leifsson, 2021; Liu et al., 2022).

### 3.2.3. CFD DDS

For the referenced works, the problem of building a DDS based on the data generated as described in Section 3.2.3 can be considered a conventional ML multi-output regression problem (Shalev-Shwartz and Ben-David, 2014). In this context the inputs of the regression problem are the vector of parameters that characterize the geometries (Section 3.1.1) and the outputs are the desired KPIs to estimate (Section 3.1.3).

The ML pipeline to address a multi-output regression problem consists of three main parts

- data-cleaning and data normalization (Hastie et al., 2001; Clarke et al., 2009; Ilyas and Chu, 2019; Fahrholz and Caprace, 2022; Guerrero et al., 2018);
- model development (Goodfellow et al., 2016; Shawe-Taylor and Cristianini, 2004; Shalev-Shwartz and Ben-David, 2014; Massaro and Benini, 2015; Huang and Yang, 2016; Bonfiglio et al., 2018; Ou et al., 2019; Coppèdè et al., 2019; Tao and Sun, 2019; Miao and Wan, 2020; Han et al., 2020; Mittendorf and Papanikolaou, 2021; Raul and Leifsson, 2021; Liu et al., 2022);
- model selection and error estimation (Oneto, 2020).

In the first phase, data are, mostly manually, explored and checked for inconsistency/outliers (Hastie et al., 2001; Clarke et al., 2009). This phase is useful to check for errors in EFD measurements or failures in CFD simulations (Fahrholz and Caprace, 2022; Guerrero et al., 2018). Subsequently, to avoid numerical issues, data is normalized.

In the second phase, a series of algorithms, shallow and/or deep, are chosen together with the range of their hyperparameters to learn the input–output relation (Goodfellow et al., 2016; Shawe-Taylor and Cristianini, 2004; Shalev-Shwartz and Ben-David, 2014). In this setting, shallow models are preferred since they are less data-hungry (Liu and

Lang, 2019; Horwath et al., 2020) and better suited for the tabular data that mostly characterizes the problem at hand (Massaro and Benini, 2015; Huang and Yang, 2016; Bonfiglio et al., 2018; Ou et al., 2019; Coppedè et al., 2019; Miao and Wan, 2020; Han et al., 2020; Mittendorf and Papanikolaou, 2021; Raul and Leifsson, 2021; Liu et al., 2022). When input data are more structured (e.g., the input represents the actual 2D or 3D geometries), or we have a huge amount of data, deep models are preferred (Wang et al., 2023; Achour et al., 2020; Wang et al., 2022b).

The third and final step is the model selection and error estimation phase (Oneto, 2020). Model selection is devoted to the selection of the optimal algorithms and associated hyperparameter (Oneto, 2020; Huang and Yang, 2016; Coppedè et al., 2019; Coraddu et al., 2020) while error estimation is devoted instead to providing an estimation of the future performance of the final model learned with the best optimal algorithms and associated hyperparameter on the available data (Oneto, 2020; Coraddu et al., 2020).

In the following paragraphs, we will review the use of shallow and deep models and how model selection and error estimation are actually performed in the current literature. We will not focus on data-cleaning and data normalization since this part is heavily handcrafted and usually not detailed in the works.

**Shallow models.** Gaussian Processes Regression (GPR) were leveraged in Bonfiglio et al. (2018), Coppedè et al. (2019), Han et al. (2020), Mittendorf and Papanikolaou (2021), Ou et al. (2019), Tao and Sun (2019), Wang et al. (2020) and Raul and Leifsson (2021) and specifically the Kriging algorithm (which is a type of GPR) was seen in Mittendorf and Papanikolaou (2021), Han et al. (2020), Wang et al. (2020) and Raul and Leifsson (2021). For what concerns the problem at hand, this approach treats the model parameters as random variables and thus determines a probability distribution for each parameter (Bolstad, 2007). Since GPR is non-parametric, this approach is not concerned with the ability of a single function to fit the data but instead calculates the probability distributions according to all of the functions that can fit the data (Rasmussen and Williams, 2006). This means we have to specify a prior to bound the specific functions we consider. For the case of GPR, the prior distribution is a Gaussian (Neal, 1998). The posterior distribution is then obtained by looking at the data and determining the probability distribution based on Bayes' theorem (Rasmussen and Williams, 2006). In Coppedè et al. (2019), Mittendorf and Papanikolaou (2021) and Ou et al. (2019) the authors opt to use the Radial Basis Function (RBF) with two hyperparameters (Schulz et al., 2018):  $\lambda$  (the length-scale) and  $\sigma^2$  (the signal variance), to map the data into a higher dimensional space where a linear solution exists to the problem at hand. Kriging and GPR are interpolation algorithms based on Gaussian processes and focused on fitting a function into every point in the data. For the construction of a DDS, the fact GPR passes through every point in the data set may be a useful attribute when the learning paradigm is focused within the bounds of the data (*in re* interpolation scenario as discussed in Section 2). On the other hand, this characteristic may pose some problems when it comes to extrapolating outside the training data in comparison to algorithms that are designed to generalize (the extrapolation approach). In the referenced works, which mostly addressed constructing the DDS to interpolate within the bounds of the database, the accuracy of the models was often characterized by 1% of Relative Error in Percentage (REP) and  $R^2 \geq 0.9$  (Bonfiglio et al., 2018; Coppedè et al., 2019) which suggests this approach is well suited for interpolating within the bounds of the experiments even when dealing with very complex functions.

Kernel methods (Shawe-Taylor and Cristianini, 2004), were used in Huang and Yang (2016), Mittendorf and Papanikolaou (2021) and Walker et al. (2024). Kernel Ridge Regression (KRR) was used in Huang and Yang (2016) and Walker et al. (2024). Additionally, Support Vector Regression (SVR) (Cortes et al., 1995) was leveraged in Mittendorf and Papanikolaou (2021). In both KRR and SVR it is possible

to exploit kernel functions to learn a model for very complex functions (Fernández-Delgado et al., 2014; Wainberg et al., 2016) although the kernel and model hyperparameters ( $\gamma$ ,  $\lambda$ ) (Oneto et al., 2015) must be tuned according to an appropriate MS procedure (Oneto, 2020). When kernel methods were used to construct a DDS for the interpolation scenario within the bounds of the database, the accuracy of the surrogates was similar to the Bayesian GPR with the scatter plots (Shao et al., 2017) showing a good agreement between the real versus predicted resistance (Huang and Yang, 2016; Mittendorf and Papanikolaou, 2021).

Ensemble Methods, demonstrated in Walker et al. (2024), are tree-based algorithms that group weak predictors to generate robust ensembles. Random Forest (RF) (Breiman, 2001; Orlandi et al., 2016) is based on randomly sampling a subset of the training data to build different trees and averaging the models' outputs to reduce variance and improve performance. Alternatively, XGBoost (Chen and Guestrin, 2016), in contrast to RF, builds models sequentially, where each new tree attempts to correct the errors made by the previous ones. This technique gradually leads to improved model performance.

Shallow Neural Networks (SNNs) (Goodfellow et al., 2016) are a versatile set of algorithms (Abiodun et al., 2018) that leverage different optimizers, e.g., backpropagation (BP) (Busecma, 1998), ADAM (Kingma and Ba, 2015), Levenberg-Marquard (LM) (Kumaraswamy, 2021), etc., to train models containing neurons layered in a structure that resembles the human brain (Mehrotra, 1996). Basically, SNNs are Kernel Methods where the kernel is not fixed *a priori* but learned from the data (Goodfellow et al., 2016; Aggarwal, 2018). SNNs are widely adopted for their ability to perform well even on complex functions (Hornik et al., 1989) and were used in Massaro and Benini (2015) and Tao and Sun (2019). The referenced works found that SNNs worked well with a significant proportion of samples (Massaro and Benini, 2015) and were able to learn a number of complex relationships (Massaro and Benini, 2015) but were superseded by other approaches when the number of samples was low, e.g., in Tao and Sun (2019). Another network based algorithm, based on the SNNs, is the Extreme Learning Machine (ELM) (Ding et al., 2014) used in Coraddu et al. (2020) and Walker et al. (2024). The approach of the ELM is very similar to Kernel Methods but the kernel is generated randomly (random projection) (Huang et al., 2006). In Coraddu et al. (2020), authors found the ELM was able to construct an effective DDS to predict the hydrodynamic response of a submersible substructure in both an interpolation case (working within the bounds of the data) with a Mean Absolute Percentage Error (MAPE) of 3.75% and an extrapolation case where the DDS was evaluated using data outside the scope of the original problem with a MAPE of 5.78%.

**Deep models.** Since data for shape optimization of hulls and airfoils data are quite in research, DDS based on deep models are not commonly used. A Deep Neural Network (DNN) based DDS was investigated in Tao and Sun (2019) where they used a database of 28 airfoils and reserved 4 geometries for testing. The REP using the DNN was 4.38% which was worse than using kriging (2.39%) for the DDS designed to interpolate within the boundaries of the database. However, authors of Shukla et al. (2024) demonstrated a DNN trained on the NACA airfoil dataset to predict the viscous flow field around the airfoil design. Results indicated that a highly accurate prediction can be obtained when sufficient data are available. Additionally, since the DNN is trained to predict a series of functions, it is invariant to the input space. Thanks to this particular property, authors show that the DNN can work with both low and high dimensional shape parametrizations without the need for retraining.

**Model selection and error estimation.** One of the main lacks in current research is that the model selection and error estimation phases are often undocumented or incomplete in the referenced works. This lack has been raised before in research (Coraddu et al., 2020). On occasion, authors do not report the accuracy metrics on the error estimation

which makes it difficult to evaluate the DDS (Massaro and Benini, 2015). On the other hand, some of the referenced work (Huang and Yang, 2016; Miao and Wan, 2020; Mittendorf and Papanikolaou, 2021) presented scatter plots (Shao et al., 2017) to illustrate the performance of the DDS models instead of conventional accuracy metrics. In the referenced works, different statistical approaches were used for the EE: a Monte Carlo (MC) simulation was used in Huang and Yang (2016), Leave-One-Out (LOO) repetition was used in Coppedè et al. (2019), and K-Fold Cross validation (KCV) was used in Coppedè et al. (2019) and Coraddu et al. (2020).

### 3.2.4. Summary

Based on the review performed in Sections 3.2.1, 3.2.2, and 3.2.3 we reported in Table 2 the most important works which deal with Step (2) considering the main different critical and fundamental aspect that raised during the review process

- Parent Geometry: the shape subject that has been optimized;
- Sampling: the strategy exploited and the number of samples drawn from the design space;
- CFD: the method(s) used for data generation;
- DDS: the algorithm(s) exploited to build the DDS(s);
- KPI: the KPI(s) informed by the CFD and estimated by the DDS(s);
- Performance: the performance of the DDS(s).

## 3.3. Step (3) Shape optimization

Step (3) deals with mainly two aspects: the definition of the optimization problem (as previously described in Section 2) to define objectives and constraints (Section 3.3.1) and then the choice of the optimizer (Section 3.3.2). Section 3.3.3 will summarize the main work in the literature according to the most critical aspects identified during the review of the two main aspects related to Step (3).

### 3.3.1. Objectives and constraints

The optimality of particular hull or airfoil varies greatly depending on the specific application and is assessed according to a number of different KPI(s). For the reasons described in Section 1, shape optimization is usually concerned with minimizing the energy requirements of a candidate shape (Bonfiglio et al., 2018; Coppedè et al., 2019; Huang and Yang, 2016; Han et al., 2020; Mittendorf and Papanikolaou, 2021; Massaro and Benini, 2015; Ou et al., 2019; Raul and Leifsson, 2021; Lye et al., 2021; Tao and Sun, 2019). Typically, the design of the most efficient hull or airfoil is aimed at achieving minimal energy usage (i.e., efficient fuel usage) which is particularly relevant given current global considerations (Yilmaz, 2022; Sala et al., 2022). Therefore, when it comes to the objectives of shape optimization of hulls and airfoils we are mostly concerned with minimizing the drag of a hull (Campana et al., 2006; Tahara et al., 2006; Kostas et al., 2015; Huang and Yang, 2016; Cheng et al., 2018; Coppedè et al., 2019; Miao and Wan, 2020; Wang et al., 2020; Zhang et al., 2021b; Mittendorf and Papanikolaou, 2021; Liu et al., 2022) or the lift and drag of an airfoil (Koziel and Leifsson, 2013; Massaro and Benini, 2015; Zhang et al., 2016; Herrema et al., 2017; Ou et al., 2019; He et al., 2019; Tao and Sun, 2019; Shi et al., 2020; Han et al., 2020; Du et al., 2021; Lye et al., 2021; Raul and Leifsson, 2021; García-Gutiérrez et al., 2022). However, in addition to energy efficiency, various studies consider optimality through the lens of maximizing safety (Ou et al., 2019) and performance (Raul and Leifsson, 2021; Ou et al., 2019).

Considering the constraints applied to CFD DDS-based shape optimization of hulls and airfoils, researchers and practitioners often prefer to bound the optimization problem with simple box constraints (Massaro and Benini, 2015; Ou et al., 2019; Coppedè et al., 2019; Tao and Sun, 2019; Han et al., 2020; Lye et al., 2021; Mittendorf and Papanikolaou, 2021; Raul and Leifsson, 2021; Liu et al., 2022). This is certainly a feasible approach when the parameter ranges are small (Ou et al., 2019; Coppedè et al., 2019; Liu et al., 2022). However, this is

often not possible when the shape design space is quite large and filled with unfeasible or inadmissible shapes, because of the approximations during the parametrization (see Section 3.1.1) (Massaro and Benini, 2015; Zhang et al., 2016; Huang and Yang, 2016; Herrema et al., 2017; Bonfiglio et al., 2018; Coppedè et al., 2019; Ou et al., 2019; Tao and Sun, 2019; Shi et al., 2020; Han et al., 2020; Du et al., 2021; Lye et al., 2021; Raul and Leifsson, 2021; Liu et al., 2022). Therefore, additional constraints are imposed based on the physical properties of the parent geometry (e.g., thickness) or problem under exam (e.g., Angle of Attack - AoA and static stability) (Massaro and Benini, 2015; Huang and Yang, 2016; Bonfiglio et al., 2018; Tao and Sun, 2019; Miao and Wan, 2020; Han et al., 2020; Mittendorf and Papanikolaou, 2021; Raul and Leifsson, 2021; Hu et al., 2022). Imposing constraints based on the physical properties of the shape was shown to be particularly important when dealing with parametrizations based on non-physical descriptors (e.g., FFD) (Huang and Yang, 2016; Miao and Wan, 2020).

### 3.3.2. Optimizers and performance

When it comes to the choice of optimizer the state-of-the-art approaches for CFD DDS-based shape optimization belong to, broadly speaking, three main categories (Ruder, 2016; Poli et al., 2007; Vikhar, 2016): (i) Gradient-based Algorithms (Ruder, 2016), (ii) Swarm Intelligence Algorithms (Poli et al., 2007), (iii) Evolutionary Algorithms (Vikhar, 2016).

Nevertheless, the Shape Optimization of Hulls and Airfoils problem mainly results in a mixed-integer, non-convex objective, and non-linearly constrained optimization problems (Massaro and Benini, 2015; Zhang et al., 2016; Huang and Yang, 2016; Herrema et al., 2017; Bonfiglio et al., 2018; Coppedè et al., 2019; Ou et al., 2019; Tao and Sun, 2019; Miao and Wan, 2020; Shi et al., 2020; Han et al., 2020; Du et al., 2021; Lye et al., 2021; Raul and Leifsson, 2021; Mittendorf and Papanikolaou, 2021; Liu et al., 2022) that reduces the choices for optimizer selection (Ruder, 2016; Poli et al., 2007; Vikhar, 2016).

Regarding Evolutionary Algorithms (Vikhar, 2016), Genetic Algorithms (GAs) (Liu et al., 2022) and variants (Massaro and Benini, 2015; Ou et al., 2019; Coppedè et al., 2019; Miao and Wan, 2020; Mittendorf and Papanikolaou, 2021; Walker et al., 2024), are far and beyond the most popular algorithm in the literature for solving hull and airfoil shape optimization problems. Investigations utilizing GAs show they are particularly effective in mixed-integer, non-convex, and non-linearly constrained problems, common in hull and airfoil optimization (Massaro and Benini, 2015; Ou et al., 2019; Coppedè et al., 2019; Miao and Wan, 2020; Mittendorf and Papanikolaou, 2021). The core strength of GAs lies in their evolutionary-inspired mechanism to explore a broad spectrum of possible candidate designs. This approach iteratively generates new candidates by combining characteristics from existing designs in the population (Vikhar, 2016). The effectiveness of this strategy to find optimal designs is shown in the referenced works leveraging GAs, which found significant performance improvements of 7 ÷ 10% (Bonfiglio et al., 2018; Coppedè et al., 2019; Miao and Wan, 2020). However, while evolutionary strategies are proven to be effective, this success comes with a price. In fact, new candidate designs are introduced within the shape optimization by means of combining traits from existing designs in the population. This strategy leads to a generating a significant proportion of infeasible and sub-optimal designs due to the complex relationship between the shape design parameters and the candidate's performance. For this reason, GAs can be computationally demanding and may require significant time to converge, especially in complex, multi-dimensional search spaces such as with the problem at hand.

Regarding Swarm Intelligence Algorithms (Poli et al., 2007), such as Particle Swarm (Tao and Sun, 2019) and Artificial Bee Colony (Huang and Yang, 2016) optimization, were also demonstrated to be a popular and effective choice for solving hull and airfoil shape optimization problems. These algorithms also excel in exploring complex search

**Table 2**

Most important works which deal with Step (2) considering the shape subject that has been optimized (Parent geometry), the sampling strategy exploited and the number of samples sampled (Sampling), the CFD method(s) used for data generation (CFD), the algorithm(s) exploited to build the DDS(s) (DDS), the KPI(s) informed by the CFD and estimated by the DDS(s) (KPI), and the performance of the DDS(s) (Performance).

Ref.	Parent geometry	Sampling	CFD	DDS	KPI	Performance
Massaro and Benini (2015)	Airfoil	320 samples drawn from 8 generations of optimization	Initial population of points evaluated using RANS Solver (500 × 150 mesh) Spalart-Allmaras turbulence for an SC1095 helicopter blade.	SNN	Cl	–
Huang and Yang (2016)	Hull	200 samples drawn from LHS DoE	CFD simulations and Steady Ship Flow solver based on Neumann-Michell validated against other literature.	RBF Interpolation and Multi- quadratic kernel method	Drag	Cross-validated scatter plot shows agreement between CFD model and DDS.
Bonfiglio et al. (2018)	Hydrofoil	1100 samples made up of 1000 LF and 100 HF simulations drawn from LHS DoE	URANS CFD performed in OpenFOAM and validated on experimental data. LF coarse grid simulations (0.5M cells) and HF fine grid simulations (3.5M cells).	GPR Kriging model with Matern 5/2 kernel.	Drag	DDS error of approximately 1% from HF model.
Ou et al. (2019)	Airfoil	25 samples drawn from OS DoE	2d RANS CFD model in ANSYS Fluent with k-w SST turbulence and ICEM mesh with 129÷143k cells.	DDS with Quadratic Response Surface Method developed in Isight 5.5	Cd & Q	R2 = 0.964 for Cd and 0.965 for Q.
Coppedè et al. (2019)	Hull	30÷90	RANS CFD in OpenFOAM with a mesh containing 2.5 × 10 <sup>6</sup> elements. Mesh validated against workshop averages.	GPR Response Surface Method.	Drag	LOO resampling R2 = 0.947÷0.973; RMSE = 0.09÷0.05 for DDS.
Tao and Sun (2019)	Airfoil	5 samples for HF approach and 19 for LF drawn out of design space sampled with Gibbs sampling method.	CFD RANS model with 22 m cells for HF approach and k-w SST turbulence for LF. Models validated against experimental data with 0.88÷1.89 % error between physical and virtual.	SNN (BP), Kriging, DBN, and Multi-Fidelity DBN	Cd at Ma = [0.765, 0.775, 0.785, 0.795, 0.805]	DDS Errors: BP 5.91% Kriging 4.71% DBN 4.38% Multi-Fidelity DBN 2.39%.
Miao and Wan (2020)	Hull	40 samples chosen from LHS DoE	CFD RANS and NM. Models validated against experimental results and maximum error is 2.45%.	RBF Interpolation, SVR, and MARS	Drag at Fr = [0.2, 0.26]	LOO cross-validation showed good agreement between experiment and DDS prediction.
Han et al. (2020)	Airfoil	2105 samples across 3 levels of fidelity using LHS DoE	HF model with 131k cells; MF model with 33k cells; and LF model with 8k cells.	Multi-hierarchical Kriging (MHK) with varied numbers of samples for each fidelity model.	Drag	Error of 0.008% at 46% reduction in CD; MHK DDS outperforms regular kriging.
Lye et al. (2021)	Airfoil	544 samples (N0 + kΔN training samples, for N0 = 64 and ΔN = 16, k up to 30)	Euler equations using NUWTUN finite volume solver for RAE2822 wing solved for steady-state convergence using implicit time scheme.	DNN	Cl & Cd	–
Mittendorf and Papanikolaou (2021)	Hull	2000 samples drawn from LHS DoE in 6 dimensions.	CFD using FreSCO+ solver with HF RANSE model with 2.1 m cells used to develop LF in-house Rankine-panel method for reduced computational time. Final models validated on HF RANS models and sit within ±2% error bounds.	GPR, SVM, MARS	Drag	–

(continued on next page)

spaces, but in a fundamentally different way to evolutionary approaches. Rather than combining different traits of candidates to form new designs, Swarm Intelligence Algorithms leverage the collective behavior of a group of individuals or particles. In the case of Particle Swarm Optimization, each particle adjusts its position in the search space based on its own experience and the best experiences of its neighbors, mimicking the behavior of a flock of birds (Poli et al., 2007). On the other hand, Artificial Bee Colony Optimization, is inspired by the foraging behavior of honey bees, where a number of potential solutions are explored and the information is shared within the optimization (Thiruganasambandam et al., 2022). The advantage

of Swarm Intelligence Algorithms is the ability to quickly converge to promising regions in the search space due to the collaboration among individuals or particles. The referenced works found performance improvements on 10 ÷ 15% (Huang and Yang, 2016). However, Swarm Intelligence Algorithms have been noted to struggle in cases where the search space is highly non-convex or contains multiple local optima (Goel, 2020).

Finally, regarding Gradient-based optimizers (Bonfiglio et al., 2018; Han et al., 2020; Lye et al., 2021; Raul and Leifsson, 2021), it is worth mentioning that these algorithms are typically preferred for learning the weights of ML algorithms rather than solving hull and airfoil shape

Table 2 (continued).

Ref.	Parent geometry	Sampling	CFD	DDS	KPI	Performance
Raul and Leifsson (2021)	Airfoil	60÷80 drawn from LHS DoE	CFD RANS model in OpenFoam of NACA0012 wing with BlockMesh utility and 387k cells. Model validated against literature (LES and EFD) and full grid and time independence studies conducted to validate spatial and temporal resolutions.	Kriging	Stall angle	RNMSE: 10% for DDS to predict objective and >5% for constraint.
Liu et al. (2022)	Hull	20÷50 drawn with Sobol sampling	CFD RANS model in (naoe-FOAM)/NMSHIP-SJTU with a mesh using 3 coarseness levels. Grid independence study and experimental validation reported to validate CFD models.	(Co-)Kriging	Drag	DDS RMSE: 0.7÷0.45 using 20÷50 samples. Results show mixed fidelity (HF + LF) DDS did not always outperform single-fidelity model.
Walker et al. (2024)	Hull	FF DoE	CFD RANS model in StarCCM+ with a grid quality assessment. Validation of CFD with experimental results is reported.	RF, XGBoost, KRR, ELM	Drag at both high and low speeds.	DDS MAE = 0.9 ÷ 1.8[N] based on increasingly complex LOO extrapolation scenarios.
Luo et al. (2021)	Hull	Optimal LHS DoE	CFD RANS model in Ansys Fluent with a grid quality assessment. Validation of CFD with experimental results is reported.	RBF	Drag and Energy Consumption	DDS R2 = 0.99 for Drag and 0.97 for Energy Consumption reported on 10 samples.
Wan et al. (2022)	Hull	60 samples drawn from LHS DoE for 2 scenarios (120 total samples)	CFD RANS model in StarCCM+. Grid independence study with 3 levels of mesh coarsening reported.	4th-order Response Surface Method	Drag at surface and underwater at 0.42 m	DDS R2 = 0.97 and 0.95 respectively.
Hu et al. (2022)	Airfoil	500 samples drawn from LHS DoE	CFD RANS model in StarCCM+. Grid independence study with 3 levels of mesh coarsening reported for 3 different KPIs. Final CFD model is also validated with experimental results.	ANN	Lift to Drag ratio and static-stability height	DDS MSE = 0.05 averaged over the 2 outputs.
Zhang et al. (2021a)	Underwater glider	70 samples drawn from LHS DoE	CFD RANS model in Fine/Marin. Grid independence study with 2 levels of coarsening is reported.	Kriging	Lift to Drag ratio	–

optimization problems. However, in the referenced works, they were shown to be an effective choice for some problems (Bonfiglio et al., 2018; Han et al., 2020; Lye et al., 2021), leading to performance increases of 7 ÷ 50. Although, it is fair to say that the shape optimization problems considered in this review are not convex, so it is worth mentioning that this approach relies on relaxing the shape optimization problem, either globally or in iterative local stages, into a convex formulation (Ruder, 2016). Global relaxation is usually not preferred due to the fact this approximation leads to a severe penalty on the accuracy of solving the problem. Therefore, local-convexity is assumed and the optimization is repeated using a multi-start strategy to find a global optimal (Raul and Leifsson, 2021). Although, it is worth mentioning that dealing with the local-convexity approximation with multi-start may lead to significant computational overhead due to performing a large number of simulations.

It is worth mentioning that stochastic optimizers, e.g., Adaptive Simulated Annealing (ASA) (Luo et al., 2021) and Interval Optimization (Wan et al., 2022), are also found in the relevant literature. These algorithms leverage randomness to explore the search space effectively, making them particularly useful for complex, non-convex, and multimodal optimization. In the referenced work, to improve computational efficiency, the ASA approach is coupled with a gradient-based approach, the modified method of feasible direction (MMFD), to improve

computational efficiency (Luo et al., 2021). The interval optimization approach is based on taking into account a range of accuracy of the DDS. It was shown under certain conditions (e.g., a small interval [95% ÷ 105%]) to outperform GA-based techniques; however, larger intervals of ±10% and ±15% did not outperform GA.

Regardless of the choice of optimizer, not all of the possible solutions found during Step (3) are actually meaningful. In fact, we are only interested in the solutions that are not dominated by any other one according to at least one objective of shape optimization problem (Liu et al., 2021; Massaro and Benini, 2015), which are identified via the Skyline operator (Liu et al., 2021). Therefore, the meaningful output of Step (3) is actually a Pareto Front of candidate designs that represent all feasible solutions to the optimization depending on the priority of different objectives (Emmerich and Deutz, 2018; Massaro and Benini, 2015). In one sense, all of the solutions on the Pareto front are actually optimal according to a specific trade-off between objectives. In rare cases, often with few objectives, it may be that one solution far outperforms the rest, i.e., the Pareto frontier is formed of only one feasible solution, namely a global optimal solution. However, it is more common that the design preferences of human experts guide a selection of one or more candidate designs from the Pareto front to take into Step (4) depending on the specific application (Miao and Wan, 2020).

### 3.3.3. Summary

Based on the review performed in Sections 3.3.1 and 3.3.2 we reported in Table 3 the most important works which deal with Step (3) considering the main different critical and fundamental aspect that raised during the review process

- Parent Geometry: the shape subject that has been optimized;
- Objectives: the objective(s) that have been selected;
- Constraints: the constraint(s) that have been implemented;
- Optimizer: the optimization algorithm(s) that have been exploited;
- Performance: the achieved results in terms of improvement of the KPI(s)

### 3.4. Step (4) Physical plausibility and feedback

Step (4) deals with the validation of the final output of the optimizer in terms of physical plausibility and provides feedback to the preceding steps (e.g., to decide if the candidate design meets the specified criteria). Note that, in practical applications, this is likely the most important step of the four, but it also involves more human feedback, making it the most challenging to automate (Huang and Yang, 2016; Bonfiglio et al., 2018; Ou et al., 2019; Coppedè et al., 2019; Tao and Sun, 2019; Miao and Wan, 2020; Han et al., 2020; Lye et al., 2021; Mittendorf and Papanikolaou, 2021; Raul and Leifsson, 2021; Liu et al., 2022).

The validation in terms of physical plausibility is an important step in the pipeline since, using particular parametrization, KPIs computation, constraints, and especially DDS we are making an approximation of the physics (CFD) (Kalikatzarakis et al., 2023; Huang and Yang, 2016; Bonfiglio et al., 2018; Ou et al., 2019; Coppedè et al., 2019; Tao and Sun, 2019; Miao and Wan, 2020; Han et al., 2020; Lye et al., 2021; Mittendorf and Papanikolaou, 2021; Raul and Leifsson, 2021; Liu et al., 2022). Verifying that all these approximations did not induce numerical artifacts is vital (Huang and Yang, 2016; Bonfiglio et al., 2018; Ou et al., 2019; Coppedè et al., 2019; Tao and Sun, 2019; Miao and Wan, 2020; Han et al., 2020; Lye et al., 2021; Mittendorf and Papanikolaou, 2021; Raul and Leifsson, 2021; Liu et al., 2022).

If the DDS performance is a numerical artifact because a vast number of the induced geometries are not physically plausible (Castelvecchi, 2016; D'Amato et al., 2022; Kalikatzarakis et al., 2023; Coraddu et al., 2023), feedback to Step Step (1) might suggest augmenting the design space (reducing the dimensionality) to reduce these artifacts.

If the predictions from the DDS are significantly different from the CFD, the optimizer may be induced into false minima due to the imprecision of the DDS. Therefore, feedback to Step Step (2) may infer that more data is required to improve the reliability of the DDS to reduce the likelihood of numerical artifacts (Castelvecchi, 2016; D'Amato et al., 2022; Kalikatzarakis et al., 2023; Coraddu et al., 2023).

Feedback to Step Step (3) (Huang and Yang, 2016; Bonfiglio et al., 2018; Ou et al., 2019; Coppedè et al., 2019; Tao and Sun, 2019; Miao and Wan, 2020; Han et al., 2020; Lye et al., 2021; Mittendorf and Papanikolaou, 2021; Raul and Leifsson, 2021; Liu et al., 2022; Koziel and Leifsson, 2013; Huang and Yang, 2016; Feng et al., 2018; Massaro and Benini, 2015) may infer that the dimensionality of the parametrization is too small, and more free variables are required to find an optimal design. Similarly, the box constraints on the parametrization may be improved to facilitate exploring a larger number of candidate designs. Another feedback could be to change the optimizer hyperparameters if the solutions found are sub-optimal.

Based on the review performed in this section, we reported in Table 4 the most important works which deal with Step (4) considering

- Parent Geometry: the shape subject that has been optimized;
- Physical Plausibility: the adopted method to check for the physical plausibility of the generated geometry.

## 4. Open problems and future perspectives

Following the review carried out in Section 3, this section elaborates on the open problems of future perspectives of the shape optimization of hulls and airfoils leveraging CFD and DDSs.

Regarding Step (1), it is clear from the review that each work develops a unique parametrization schema (e.g., particularly when using domain-based parametrizations) requiring a new database to be collected/generated from EFD and CFD simulations. While this problem is overcome by standardized parametrizations (e.g., Hicks-Henne and PARSEC-11), there is a lack of standardized schemes for domain-based parametrizations. The latter represents an important open challenge (especially for hull shape optimization). Establishing a new database for every parametrization scheme presents a considerable challenge, as it greatly increases computational costs and necessitates human oversight. This issue is further complicated when devising a dedicated parametrization scheme alongside CFD models. Additionally, such a high degree of customization poses a significant hurdle for the community in terms of developing shared datasets. These shared resources are crucial for continually expanding toward larger and more diverse design spaces. Decoupling parametrization from parameters leveraged by DDSs to make prediction (Walker et al., 2024; Lazarevska, 2018; Šegota et al., 2021; Fahrholz and Caprace, 2022; Shukla et al., 2024) may help the community in reusing the same DDSs in optimization with different parametrization schema.

Regarding Step (2), the DDS models reviewed in this work show the learning paradigm is almost always focused on interpolating rather than extrapolating beyond the bounds of the data used to construct the models. This means that little effort has been made to assess the performance of DDS models with a specific setting or application. In fact, there are a number of interesting extrapolation scenarios (unseen families of geometries, unseen geometries, or unseen speeds) that are useful to develop models that work well when applied outside the boundaries of the data used to construct them (Walker et al., 2024). Extrapolation is a particularly valuable attribute of DDS models since, in practice, shape optimization is the adaptation of an existing (not optimized) design for specific KPIs. Existing designs for hulls and airfoils are based on historical design requirements (e.g., using conventional fuels), and changing design requirements (inspired by fluctuations in fuel prices or addressing climate change) requires exploring a wider design space leveraging DDS models that remain accurate even in extrapolating conditions. Hence, during DDS-based shape optimization it is beneficial to produce a geometry for novel, yet-to-be-explored candidates, rather than confining ourselves to established (not optimized) designs.

Regarding Step (3), the current approach to optimization largely relies on well established methods for solving multi-objective non-linear and non-linearly constrained problems. Given the context of increased design uncertainty for hulls and airfoils, there is a necessity for a more comprehensive exploration of certain aspects within the domain of shape optimization. One promising avenue to achieve this is the cross-fertilization of methodologies from operations research into this field of research. State-of-the-art techniques from operations research and other related fields, such as physics-based optimization and hybrid strategies (Mohammadi and Sheikholeslam, 2023), offer a number of methods to enhance the current approaches to optimization in CFD-DDS based shape optimization of hulls and airfoils. Moreover, the increase in quantum computing resources presents an opportunity for enhanced optimization methods in the future. Quantum computers, which can perform complex computations at speed, offer the potential to reduce the time required for optimization tasks (Meglio et al., 2023). The integration of these advanced computational techniques with existing CFD DDS shape optimization could lead to significant breakthroughs in the field.

Finally, regarding Step (4), there are a number of instances in the referenced works where the validation of the candidate designs is not confirmed using the high-fidelity CFD. This remains an open problem

**Table 3**

Most important works which deal with Step (3) considering the shape subject that has been optimized (Parent geometry), the objective(s) that have been selected (Objectives), the constraint(s) that have been implemented (Constraints), the optimization algorithm(s) that have been exploited (Optimizer), and the achieved results in terms of improvement of the KPI(s) (Performance).

Ref.	Parent geometry	Objectives	Constraints	Optimizer	Performance
Massaro and Benini (2015)	Airfoil	Minimize $C_L$ in two conditions with different free-stream velocities and angles of attack.	Geometrical constraint to ensure thickness $> 9.5\%$ .	GA variant	No improvement found from baseline geometries after 20 generations.
Huang and Yang (2016)	Hull	Minimize total Drag over 3 Froude Numbers.	DDS developed for displacement constraint.	Artificial Bee Colony	Optimizer found a 10 ÷ 15% reduction in Drag for low and high speeds.
Bonfiglio et al. (2018)	Hydrofoil	Minimize ratio of $c_D/c_L$ to the $c_D/c_L$ ratio of a benchmark solution.	Constrained $0.09 \leq C_L \leq 0.11$ and geometric constraint on thickness.	Gradient Descent	Improved performance by 7%
Ou et al. (2019)	Airfoil	Minimize the $C_D$ and the Heat flux ( $Q$ ).	Box constraints on parameter ranges.	GA variant	Optimal designs found for single- and multi-objective problems.
Coppedè et al. (2019)	Hull	Minimize the Drag.	Box constraints on parameter ranges.	GA variant	Optimal candidate found by optimizer and DDS reduced Drag by 3N (8%).
Tao and Sun (2019)	Airfoil	Minimize the Drag at 3 Mach numbers.	Geometric constraints on AoA and wing thickness at different points.	Particle Swarm	Optimal candidate found that outperformed the baseline geometry.
Miao and Wan (2020)	Hull	Minimize the Drag at two Froude numbers.	Geometric constraints fix main dimensions of the hull. Additionally, maximum variation for displacement and surface area is fixed at $\pm 1\%$ .	GA variant	3 Pareto-optimal candidates selected with 5 ÷ 10% reduction in drag according to the DDS.
Han et al. (2020)	Airfoil	Minimize $C_L$	$C_D \geq C_L$ of baseline geometry. Thickness constraints over the width of the design.	Gradient-based	Cd reduced between 23 ÷ 25% according to DDS models developed with varying fidelity data.
Lye et al. (2021)	Airfoil	Minimize $C_D$	$C_L$ is kept constant according to a benchmark design (around 0.9). Strict penalty on deviating $C_L$ constrains the shape design space around the reference airfoil.	Gradient-based	Optimal candidate found with very similar $C_L$ (0.88) and 50% reduction in $C_D$ .
Mittendorf and Papanikolaou (2021)	Hull	Minimize Drag at 5 speeds.	Constant displacement.	GA variant	At design speed of 23 knots DDS models predicted reduction in drag of 1 ÷ 1.5%.
Raul and Leifsson (2021)	Airfoil	Minimize dynamic stall.	Constrained the dynamic stall point of the airfoil shape (informed by a DDS).	Gradient-based	Optimized airfoil increased stall angle by 3°
Liu et al. (2022)	Hull	Minimize Drag	Box constraints on parameter ranges.	GA	Drag reduced by 4N with single-fidelity DDS and 2N with mixed-fidelity DDS.
Walker et al. (2024)	Hull	Minimize weighted sum of Drag at high and low speeds	Box constraints on parameter ranges.	GA variant	Significant Drag reductions found based on the extent of variation from the baseline design.
Luo et al. (2021)	Hull	Minimize weighted sum of Drag and Energy Consumption	Box constraints on parameter ranges.	ASA+MMFD	Drag reduced by 9 ÷ 11% and Energy Consumption by 3 ÷ 4%.
Wan et al. (2022)	Hull	Minimize Drag	Box constraints on parameter ranges.	GA and Interval Optimization.	Drag reduced by 4% and 6% with GA and Interval Optimization respectively.
Hu et al. (2022)	Airfoil	Maximize Lift over Drag	Box constraints on parameter ranges.	GA	Lift to Drag ratio decreased compared to baseline design due to static stability constraint.
Zhang et al. (2021a)	Underwater glider	Maximize Lift over Drag	Box constraints on parameter ranges.	GA	Lift to Drag ratio increased by 18.98% compared to baseline design.

**Table 4**

Most important works which deal with Step (4) considering the shape subject that has been optimized (Parent geometry) and the adopted method to check for the physical plausibility of the generated geometry (Physical Plausibility).

Ref.	Parent geometry	Physical Plausibility
Huang and Yang (2016)	Hull	Validation with numerical (CFD) and experimental (EFD) methods showed candidate shape increased drag by 6% at low speeds and decreased drag between 6 ÷ 13% at medium to high speeds.
Bonfiglio et al. (2018)	Hydrofoil	Validation with LF and HF solvers informed the candidate shape performance.
Ou et al. (2019)	Airfoil	Validation of the candidate design with CFD showed the $C_D$ predicted by the optimizer was 7% lower than the HF model and 1% lower for $Q$ .
Coppedè et al. (2019)	Hull	Validation with CFD showed the optimal candidate had a Drag reduction of 0.5N (1%).
Tao and Sun (2019)	Airfoil	Validation showed good agreement between CFD and DDS predicted $C_D$ for the optimal candidate.
Miao and Wan (2020)	Hull	Results validated with NM plus CFD method and pressure distribution around the candidates compared to original for plausibility.
Han et al. (2020)	Airfoil	Validation with CFD showed good agreement with DDS. Error of DDS prediction on optimal candidate was 0.2 ÷ 0.5%.
Lye et al. (2021)	Airfoil	Validation shows physical plausibility and explains large reduction in $C_D$ by reducing in upper shock on upper surface.
Mittendorf and Papanikolaou (2021)	Hull	Final design validated with HF RANS model showed 1 design failed physical plausibility (drag actually increased) and the other passed (error between DDS and CFD of 0.4%).
Raul and Leifsson (2021)	Airfoil	Final model validated against HF CFD showed physical plausibility.
Liu et al. (2022)	Hull	Validation with HF CFD showed actual reduction of 1N for single-fidelity candidate and agreement with mixed-fidelity prediction.
Walker et al. (2024)	Hull	Validation with HF CFD showed strong physical plausibility between DDS and real Drag when close to known designs. As the hull design deviated from known examples physical plausibility decreased.
Hu et al. (2022)	Airfoil	Validation with HF CFD showed 3.6% deviation between DDS and real Lift to Drag ratio and 0.0\$ error for stability prediction.
Zhang et al. (2021a)	Underwater glider	Validation with HF CFD affirmed that the actual Lift to Drag ratio outperformed the baseline design.

in the field until this procedure is common practice and must include a comparison between the KPI predicted by the DDS and the real one informed by the CFD. Ultimately, this approach will lead to a better understanding of the performance of DDS models.

## 5. Conclusion

This paper reviews the current research in shape optimization of vessel hulls and airfoils, which is a critical step to ensure optimal performance and minimal environmental footprint. In fact, their design is usually an adaptation of an existing one, not optimized for specific KPIs like the drag of a hull or lift and drag of an airfoil or the result of a mix between human experience and numerical optimization approaches. Nowadays, the state-of-the-art approach for shape optimization of hulls and airfoils is based on CFD DDS models and consists of four steps. First, parametrization and parameter ranges are defined, with more or less human intervention, to build a shape design space.

Accurate estimation of KPIs, such as drag resistance for hull designs or lift and drag for airfoils, is a cornerstone of modern aerodynamic and hydrodynamic engineering. However, the direct computation of these KPIs based on shape parameters involves complex simulations using CFD, which is notably resource intensive. This high computational demand traditionally limits the feasibility of direct numerical optimization of these KPIs in real-time design workflows. To address this challenge, a pragmatic approach is typically employed, involving a multi-step process that integrates both human expertise and advanced data-driven strategies. Initially, a selective sampling of distinct and representative shapes from the design space is conducted. This selection can be based on experienced human judgment or through sophisticated algorithmic strategies that aim to cover the potential variability in the design space. These selected designs are then subjected to detailed CFD analysis to evaluate their performance against the desired KPIs. Based on the insights gained from these analyses, a DDS model is developed. While the initial creation of the DDS is computationally demanding – requiring substantial data processing and model training – the resultant model offers a significant reduction in computational expense for subsequent predictions. This efficiency is achieved by approximating

the complex relationships between shape parameters and their resultant KPIs through learned data patterns, thus circumventing the need for direct CFD simulation in the early stages of design exploration. Recent advancements in machine learning have further enhanced the capabilities of DDS models, incorporating techniques such as deep learning and reinforcement learning to refine prediction accuracy and model robustness. Studies have demonstrated that such models can effectively predict hydro/aerodynamic properties with high reliability, approaching the fidelity of direct CFD simulations under varied operational conditions. Once the DDS is established, it can then seamlessly integrate into an optimization loop. This integration facilitates efficient exploration of the design space, enabling the rapid generation and assessment of candidate geometries. The objective is to identify designs that approximate the Pareto front, optimizing multiple conflicting KPIs simultaneously, a method that has seen significant refinement in recent years through multi-objective optimization algorithms. The final step in this process involves a rigorous validation of the proposed designs. Using CFD, the physical plausibility of each candidate geometry suggested by the DDS and the optimization framework is verified. This validation is crucial, as it ensures that the surrogate model and the optimization algorithms have not proposed non-viable or physically implausible shapes. This comprehensive evaluation not only reinforces the reliability of the DDS, but also aligns the theoretical models with practical, real-world applicability. This approach, which blends sophisticated data-driven models with traditional simulation techniques, represents a significant shift in the way hull and airfoil designs are developed. By reducing reliance on extensive CFD simulations and leveraging recent research in surrogate modeling and optimization, this methodology promises to accelerate the design cycle, reduce costs, and enhance the innovation process in fields demanding high precision and efficiency.

Based on our review, we identified several important discussion points. In general, DDS-based shape optimization is an effective strategy for the optimization of hulls and airfoils and will remain an important area of research given the current motivations towards minimizing the energy requirements of hulls and airfoils. However, a key acknowledgment is that the current approaches to parametrization (especially when using domain-based parametrizations) often lack standardization.

Consequently, much of the generated data remains unusable for future work despite a large degree of similarity among many existing designs. This redundancy not only lengthens the time frame of individual projects but also restricts the broader community's capacity to build upon prior findings. Additionally, future changes to conventional design requirements opens the door for shape optimization to explore novel design concepts, and improving the extrapolation capabilities of DDS models will significantly benefit this endeavor. However, at the time of writing, these challenges have not yet been extensively investigated or overcome.

### CRedit authorship contribution statement

**Jake M. Walker:** Writing – review & editing, Writing – original draft, Visualization, Validation, Resources, Methodology, Investigation, Formal analysis, Data curation, Conceptualization. **Andrea Coraddu:** Writing – review & editing, Writing – original draft, Visualization, Validation, Supervision, Resources, Methodology, Investigation, Formal analysis, Conceptualization. **Luca Oneto:** Writing – review & editing, Writing – original draft, Visualization, Validation, Supervision, Resources, Methodology, Investigation, Formal analysis, Data curation, Conceptualization.

### Declaration of competing interest

The authors declare that they have no known competing financial interests or personal relationships that could have appeared to influence the work reported in this paper.

### References

- Abiodun, O., Jantan, A., Omolara, A., Dada, K., Mohamed, N., Arshad, H., 2018. State-of-the-art in artificial neural network applications: A survey. *Heliyon* 4 (11), e00938.
- Acar, E., 2015. Effect of error metrics on optimum weight factor selection for ensemble of metamodels. *Expert Syst. Appl.* 42 (5), 2703–2709.
- Achour, G., Sung, W.J., Pinon-Fischer, O.J., Mavris, D.N., 2020. Development of a conditional generative adversarial network for airfoil shape optimization. In: *AIAA Scitech 2020 Forum*. p. 2261.
- Aggarwal, C.C., 2018. *Neural Networks and Deep Learning*. Springer.
- Ahmadzadehtalatapeh, M., Mousavi, M., 2015. A review on the drag reduction methods of the ship hulls for improving the hydrodynamic performance. *Int. J. Marit. Technol.* 4, 51–64.
- Albuquerque, P.F., Gamboa, P.V., Silvestre, M.A., 2018. Mission-based multidisciplinary aircraft design optimization methodology tailored for adaptive technologies. *J. Aircr.* 55 (2), 755–770.
- Altman, N., Krzywinski, M., 2018. The curse (s) of dimensionality. *Nat Methods* 15 (6), 399–400.
- Anderson, M.J., Whitcomb, P.J., 2016. *RSM Simplified: Optimizing Processes Using Response Surface Methods for Design of Experiments*, second ed. Productivity Press.
- Andersson, B., Andersson, R., Håkansson, L., Mortensen, M., Sudiyo, R., van Wachem, B., 2011. *Computational Fluid Dynamics for Engineers*. Cambridge University Press.
- Ang, J.H., Goh, C., Li, Y., 2015. Key challenges and opportunities in hull form design optimisation for marine and offshore applications.
- Antony, J., 2014. *Design of Experiments for Engineers and Scientists (Second Edition)*, second ed. Elsevier, Oxford.
- Bai, C., Wang, W., 2016. Review of computational and experimental approaches to analysis of aerodynamic performance in horizontal-axis wind turbines (HAWTs). *Renew. Sustain. Energy Rev.* 63, 506–519.
- Barnes, C.J., Visbal, M., 2016. High-fidelity LES simulations of self-sustained pitching oscillations on a NACA0012 airfoil at transitional Reynolds numbers. In: *54th AIAA Aerospace Sciences Meeting*. p. 1353.
- Bolstad, W.M., 2007. *Introduction to Bayesian Statistics*, second ed. John Wiley & Sons, Inc.
- Bonfiglio, L., Perdikaris, P., Brizzolara, S., Karniadakis, G.E., 2018. Multi-fidelity optimization of super-cavitating hydrofoils. *Comput. Methods Appl. Mech. Engrg.* 332, 63–85.
- Breiman, L., 2001. Random forests. *Mach. Learn.* 45 (1), 5–32.
- Brunton, S.L., Noack, B., Koumoutsakos, P., 2020. Machine learning for fluid mechanics. *Annu. Rev. Fluid Mech.* 52, 477–508.
- Buckley, H.P., Zhou, Y., Zingg, D.W., 2010. Airfoil optimization using practical aerodynamic design requirements. *J. Aircr.* 47 (5), 1707–1719.
- Burachik, R.S., Kaya, C.Y., Rizvi, M.M., 2022. Algorithms for generating Pareto fronts of multi-objective integer and mixed-integer programming problems. *Eng. Optim.* 54 (8), 1413–1425.
- Buscema, M., 1998. Back propagation neural networks. *Subst. Use Misuse* 33, 233–270.
- Campana, E., Peri, D., Tahara, Y., Stern, F., 2006. Shape optimization in ship hydrodynamics using computational fluid dynamics. *Comput. Methods Appl. Mech. Engrg.* 196 (1–3), 634–651.
- Casalone, P., Dell'Edera, O., Fenu, B., Giorgi, G., Sirigu, S.A., Mattiazzo, G., 2020. Unsteady RANS CFD simulations of Sailboat's hull and comparison with full-scale test. *J. Mar. Sci. Eng.* 8 (6), 394.
- Castelvecchi, D., 2016. Can we open the black box of AI? *Nat. News* 538 (7623), 20.
- Chen, T., Guestrin, C., 2016. Xgboost: A scalable tree boosting system. In: *Proceedings of the 22nd ACM SIGKDD International Conference on Knowledge Discovery and Data Mining*. ACM, pp. 785–794.
- Cheng, X., Feng, B., Liu, Z., Chang, H., 2018. Hull surface modification for ship resistance performance optimization based on Delaunay triangulation. *Ocean Eng.* 153, 333–344.
- Chicco, D., Oneto, L., Tavazzi, E., 2022. Eleven quick tips for data cleaning and feature engineering. *PLoS Comput. Biol.* 18 (12), e1010718.
- Choi, Y., Hong, S., Choi, H., 2001. An analysis of second-order wave forces on floating bodies by using a higher-order boundary element method. *Ocean Eng.* 28 (1), 117–138.
- Cipollini, F., Oneto, L., Coraddu, A., Savio, S., 2019. Unsupervised deep learning for induction motor bearings monitoring. *Data-Enabled Discov. Appl.* 3, 1–13.
- Clarke, B., Fokoue, E., Zhang, H.H., 2009. *Principles And Theory for Data Mining and Machine Learning*. Springer.
- Coppède, A., Gaggero, S., Vermengo, G., Villa, D., 2019. Hydrodynamic shape optimization by high fidelity CFD solver and Gaussian process based response surface method. *Appl. Ocean Res.* 90 (May 2018), 101841.
- Coraddu, A., Gaggero, S., Villa, D., Oneto, L., 2023. A non-deterministic propeller design optimization framework leveraging machine learning based boundary element methods surrogates. In: *International Conference on Computational Methods in Marine Engineering: MARINE2023*.
- Coraddu, A., Oneto, L., Kalikatzarakis, M., Ilardi, D., Collu, M., 2020. Floating spar-type offshore wind turbine hydrodynamic response characterisation: A computational cost aware approach. In: *2020 Global Oceans 2020: Singapore - U.S. Gulf Coast*. IEEE, pp. 1–8.
- Cortes, C., Vapnik, V., Saitta, L., 1995. Support-vector networks editor. *Mach. Learn.* 20, 273–297.
- Cui, H., Turan, O., Sayer, P., 2012. Learning-based ship design optimization approach. *Comput. Aided Des.* 44 (3), 186–195.
- D'Agostino, D., Serani, A., Diez, M., 2020. Design-space assessment and dimensionality reduction: An off-line method for shape reparameterization in simulation-based optimization. *Ocean Eng.* 197, 106852.
- D'Amato, V., Oneto, L., Camurri, A., Anguita, D., 2022. The importance of multiple temporal scales in motion recognition: when shallow model can support deep multi scale models. In: *2022 International Joint Conference on Neural Networks. IJCNN, IEEE*, pp. 01–10.
- Deb, K., 2001. *Multiobjective Optimization Using Evolutionary Algorithms*. Wiley.
- Demo, N., Tezzele, M., Gustin, G., Lavini, G., Rozza, G., 2018. Shape optimization by means of proper orthogonal decomposition and dynamic mode decomposition. In: *Technology and Science for the Ships of the Future - Proceedings of NAV 2018: 19th International Conference on Ship and Maritime Research*. pp. 212–219.
- Derksen, R.W., Rogalsky, T., 2010. Bezier-PARSEC: An optimized aerofoil parameterization for design. *Adv. Eng. Softw.* 41 (7), 923–930.
- Ding, S., Xu, X., Nie, R., 2014. Extreme learning machine and its applications. *Neural Comput. Appl.* 25, 549–556.
- Dong, G., Liu, H., 2018. *Feature Engineering for Machine Learning and Data Analytics*. CRC Press.
- Du, X., He, P., Martins, J., 2021. Rapid airfoil design optimization via neural networks-based parameterization and surrogate modeling. *Aerosp. Sci. Technol.* 113, 106701.
- Duraisamy, K., Iaccarino, G., Xiao, H., 2019. Turbulence modeling in the age of data. *Annu. Rev. Fluid Mech.* 51, 357–377.
- Emmerich, M., Deutz, A.H., 2018. A tutorial on multiobjective optimization: fundamentals and evolutionary methods. *Nat. Comput.* 17 (3), 585–609.
- Evans, J.H., 1959. Basic design concepts. *J. Am. Soc. Naval Eng.* 71 (4), 671–678.
- Fahrholz, S.F., Caprace, J.D., 2022. A machine learning approach to improve sailboat resistance prediction. *Ocean Eng.* 257, 111642.
- Feng, Y., Chen, Z., Dai, Y., Wang, F., Cai, J., Shen, Z., 2018. Multidisciplinary optimization of an offshore aquaculture vessel hull form based on the support vector regression surrogate model. *Ocean Eng.* 166, 145–158.
- Fernández-Delgado, M., Cernadas, E., Barro, S., Amorim, D., 2014. Do we need hundreds of classifiers to solve real world classification problems? *J. Mach. Learn. Res.* 15 (1), 3133–3181.
- Forrester, A., Keane, A., 2009. Recent advances in surrogate-based optimization. *Prog. Aerosp. Sci.* 45 (1–3), 50–79.
- Gain, J., Bechmann, D., 2008. A survey of spatial deformation from a user-centered perspective. *ACM Trans. Graph.* 27 (4).

- Gammon, M.A., 2011. Optimization of fishing vessels using a multi-objective genetic algorithm. *Ocean Eng.* 38 (10), 1054–1064.
- García-Gutiérrez, A., Gonzalo, J., Domínguez, D., López, D., 2022. Stochastic optimization of high-altitude airship envelopes based on kriging method. *Aerosp. Sci. Technol.* 120, 107251.
- Geirhos, R., Jacobsen, J.H., Michaelis, C., Zemel, R., Brendel, W., Bethge, M., Wichmann, F.A., 2020. Shortcut learning in deep neural networks. *Nat. Mach. Intell.* 2 (11), 665–673.
- Ghassemi, H., Zakerdoost, H., 2017. Ship hull–propeller system optimization based on the multi-objective evolutionary algorithm. *Proc. Inst. Mech. Eng. C* 231 (1), 175–192.
- Goel, L., 2020. An extensive review of computational intelligence-based optimization algorithms: trends and applications. *Soft Comput.* 24, 16519–16549.
- Goodfellow, I., Bengio, Y., Courville, A., 2016. *Deep Learning*. MIT Press.
- Guerrero, J., Cominetti, A., Pralits, J., Villa, D., 2018. Surrogate-based optimization using an open-source framework: The bulbous bow shape optimization case. *Math. Comput. Appl.* 23 (4), 60.
- Hall, W.S., 1994. Boundary element method. In: *The Boundary Element Method*. Springer Netherlands, Dordrecht, pp. 61–83.
- Han, Z., Xu, C., Zhang, L., Zhang, Y., Zhang, K., Song, W., 2020. Efficient aerodynamic shape optimization using variable-fidelity surrogate models and multilevel computational grids. *Chin. J. Aeronaut.* 33, 31–47.
- Harries, S., Abt, C., 2019. CAESSES — The HOLISHIP platform for process integration and design optimization. In: *a Holistic Approach To Ship Design*.
- Hastie, T., Tibshirani, R., Friedman, J., 2001. *The Elements of Statistical Learning*. Springer New York Inc.
- He, X., Li, J., Mader, C.A., Yildirim, A., Martins, J.R., 2019. Robust aerodynamic shape optimization—From a circle to an airfoil. *Aerosp. Sci. Technol.* 87, 48–61.
- Herrema, A.J., Wiese, N.M., Darling, C.N., Ganapathysubramanian, B., Krishnamurthy, A., Hsu, M.C., 2017. A framework for parametric design optimization using isogeometric analysis. *Comput. Methods Appl. Mech. Engrg.* 316, 944–965.
- Hicks, S.A., Isaksen, J.L., Thambawita, V., Ghouse, J., Ahlberg, G., Linneberg, A., Grarup, N., Strömke, I., Ellervik, C., Olesen, M.S., Hansen, T., Graff, C., Holstein-Rathlou, N., Halvorsen, P., Maleckar, M.M., Riegler, M.A., Kanters, J.K., 2021. Explaining deep neural networks for knowledge discovery in electrocardiogram analysis. *Sci. Rep.* 11 (1), 10949.
- Hirsch, C., 2007. *Numerical Computation of Internal and External Flows: The Fundamentals of Computational Fluid Dynamics*. Elsevier Ltd..
- Hornik, K., Stinchcombe, M., White, H., 1989. Multilayer feedforward networks are universal approximators. *Neural Netw.* 2 (5), 359–366.
- Horwath, J.P., Zakharov, D.N., Mégret, R., Stach, E.A., 2020. Understanding important features of deep learning models for segmentation of high-resolution transmission electron microscopy images. *Npj Comput. Mater.* 6 (1), 108.
- Hu, H., Zhang, G., Li, D., Zhang, Z., Sun, T., Zong, Z., 2022. Shape optimization of airfoil in ground effect based on free-form deformation utilizing sensitivity analysis and surrogate model of artificial neural network. *Ocean Eng.* 257, 111514.
- Huang, F., Yang, C., 2016. Hull form optimization of a cargo ship for reduced drag. *J. Hydrodyn.* 28 (2).
- Huang, G.B., Zhu, Q.Y., Siew, C.K., 2006. Extreme learning machine: theory and applications. *Neurocomputing* 70 (1–3), 489–501.
- Huysse, L., Lewis, R.M., 2001. *Aerodynamic Shape Optimization of Two-Dimensional Airfoils Under Uncertain Conditions*. ICASE, NASA Langley Research Center, 2001.
- Hwang, J., Martins, J.R., 2016. Allocation-mission-design optimization of next-generation aircraft using a parallel computational framework. In: *57th AIAA/ASCE/AHS/ASC Structures, Structural Dynamics, and Materials Conference*. p. 1662.
- Ilyas, I.F., Chu, X., 2019. *Data Cleaning*. Morgan & Claypool.
- Innat, M., Hossain, M., Mader, K., Kouzani, A., 2023. A convolutional attention mapping deep neural network for classification and localization of cardiomegaly on chest X-rays. *Sci. Rep.* 13 (1), 6247.
- International Maritime Organization (IMO), 2022. Sub-committee on ship design and construction (SDC). <https://www.imo.org/en/MediaCentre/MeetingSummaries/Pages/SDC-Default.aspx>.
- International Maritime Organization (IMO), 2023. *Statutory documents - IMO publications and documents - international conventions - SOLAS - international convention for the safety of life at sea - chapter II-1 - construction - structure, subdivision and stability, machinery and electrical installations*. [https://www.imo.org/en/Conventions/SOLAS\\_REGII-1.html](https://www.imo.org/en/Conventions/SOLAS_REGII-1.html).
- Jiang, P., Zhou, Q., Shao, X., 2020. *Surrogate Model-Based Engineering Design and Optimization*. Springer Singapore.
- Júnior, J.M.M., Halila, G.L., Kim, Y., Khamvilai, T., Vamvoudakis, K.G., 2022. Intelligent data-driven aerodynamic analysis and optimization of morphing configurations. *Aerosp. Sci. Technol.* 121, 107388.
- Kalikatzarakis, M., Coraddu, A., Atlar, M., Gaggero, S., Tani, G., Oneto, L., 2023. Physically plausible propeller noise prediction via recursive corrections leveraging prior knowledge and experimental data. *Eng. Appl. Artif. Intell.* 118, 105660.
- Kara, L.B., Shimada, K., 2006. Construction and modification of 3D geometry using a sketch-based interface. In: *Stahovich, T., Sousa, M. (Eds.), Eurographics Workshop on Sketch-Based Interfaces and Modeling*. The Eurographics Association.
- Keane, A., Voutchkov, I., 2020. Robust design optimization using surrogate models. *J. Comput. Des. Eng.* 7 (1), 44–55.
- Kenway, G.K., Martins, J.R., 2016. Multipoint aerodynamic shape optimization investigations of the common research model wing. *AIAA J.* 54 (1), 113–128.
- Keuning, L.J.A., Katgert, M., 2008. A bare hull resistance prediction method derived from the results of the delft systematic yacht hull series to higher speeds. In: *The International Conference Innovation in High Performance Sailing Yachts*.
- Kim, S., Boukouvala, F., 2020. Machine learning-based surrogate modeling for data-driven optimization: a comparison of subset selection for regression techniques. *Optim. Lett.* 14, 989–1010.
- Kingma, D.P., Ba, J., 2015. Adam: A method for stochastic optimization. [CoRR abs/1412.6980](https://arxiv.org/abs/1412.6980).
- Kochenderfer, M.J., Wheeler, T.A., 2022. *Algorithms For Decision Making*. MIT Press.
- Kochkov, D., Smith, J.A., Alieva, A., Wang, Q., Brenner, M., Hoyer, S., 2021. Machine learning-accelerated computational fluid dynamics. *Proc. Natl. Acad. Sci.* 118 (21).
- Kostas, K.V., Ginnis, A.I., Politis, C.G., Kakkis, P.D., 2015. Ship-hull shape optimization with a T-spline based BEM-isogeometric solver. *Comput. Methods Appl. Mech. Engrg.* 284, 611–622.
- Koziel, S., Leifsson, L., 2013. Multi-level CFD-based airfoil shape optimization with automated low-fidelity model selection. *Procedia Comput. Sci.* 18, 889–898.
- Koziel, S., Leifsson, L., 2016. *Simulation-Driven Design by Knowledge-Based Response Correction Techniques*. Springer.
- Kulfan, B., 2008. Universal parametric geometry representation method. *J. Aircr. - J. Aircr.* 45, 142–158.
- Kumaraswamy, B., 2021. Neural networks for data classification. In: *Artificial Intelligence in Data Mining*.
- Lazarevska, E., 2018. Comparison of different models for residuary resistance prediction. In: *EUROSIM Congress on Modelling and Simulation, EUROSIM*.
- Lee, K., Carlberg, K.T., 2020. Model reduction of dynamical systems on nonlinear manifolds using deep convolutional autoencoders. *J. Comput. Phys.* 404.
- Leifsson, L., Koziel, S., 2016. Surrogate modelling and optimization using shape-preserving response prediction: A review. *Eng. Optim.* 48, 476–496.
- Liu, H., Lang, B., 2019. Machine learning and deep learning methods for intrusion detection systems: A survey. *Appl. Sci.* 9 (20).
- Liu, X., Lu, P., 2014. Solving nonconvex optimal control problems by convex optimization. *J. Guid. Control Dyn.* 37 (3), 750–765.
- Liu, J., Xiong, L., Pei, J., Luo, J., Zhang, H., Yu, W., 2021. Group-based skyline for Pareto optimal groups. *IEEE Trans. Knowl. Data Eng.* 33 (7), 2914–2929.
- Liu, X., Zhao, W., Wan, D., 2022. Multi-fidelity Co-Kriging surrogate model for ship hull form optimization. *Ocean Eng.* 243, 110239.
- Luo, W., Guo, X., Dai, J., Rao, T., 2021. Hull optimization of an underwater vehicle based on dynamic surrogate model. *Ocean Eng.* 230, 109050.
- Luo, W., Lan, L., 2017. Design optimization of the lines of the bulbous bow of a hull based on parametric modeling and computational fluid dynamics calculation. *Math. Comput. Appl.* 22, 4.
- Lutz, T., Wagner, S., 1998. Drag reduction and shape optimization of airship bodies. *J. Aircr.* 35 (3), 345–351.
- Lye, K.O., Mishra, S., Ray, D., Chandrashekar, P., 2021. Iterative surrogate model optimization (ISMO): An active learning algorithm for PDE constrained optimization with deep neural networks. *Comput. Methods Appl. Mech. Engrg.* 374, 113575.
- Maniaci, D.C., Moriarty, P.J., Barone, M.F., Churchfield, M.J., Sprague, M.A., Arunajatesan, S., 2020. *Wind Energy High-Fidelity Model Verification and Validation Roadmap*. Technical Report, Sandia National Lab.(SNL-NM), Albuquerque, NM (United States).
- Marinić-Kragić, I., Vučina, D., Čurković, M., 2016. Efficient shape parameterization method for multidisciplinary global optimization and application to integrated ship hull shape optimization workflow. *Comput. Aided Des.* 80, 61–75.
- Martineau, D., Stokes, S., Munday, S., Jackson, A., Gribben, B., Verhoeven, N., 2006. Anisotropic hybrid mesh generation for industrial RANS applications. In: *Aerospace Sciences Meeting and Exhibit*.
- Massaro, A., Benini, E., 2015. A surrogate-assisted evolutionary algorithm based on the genetic diversity objective. *Appl. Soft Comput.* 36, 87–100.
- Masters, D.A., Taylor, N.J., Rendall, T.C.S., Allen, C.B., Poole, D.J., 2017. Geometric comparison of aerofoil shape parameterization methods. *AIAA J.* 55 (5), 1575–1589.
- McCall, J., 2005. Genetic algorithms for modelling and optimisation. *J. Comput. Appl. Math.* 184 (1), 205–222.
- Meglio, A.D., Combarro, E.F., González-Castillo, S., Meglio, A.D., 2023. A practical guide to quantum machine learning and quantum optimization: Hands-on approach to modern quantum algorithms.
- Mehrotra, K., 1996. *Artificial Neural Networks*. MIT Press.
- Miao, A., Wan, D., 2020. Hull form optimization based on an nm+cfD integrated method for KCS. *Int. J. Comput. Methods* 17 (10), 1–14.
- Min, K., Kang, S., 2010. Study on the form factor and full-scale ship resistance prediction method. *J. Mar. Sci. Technol.* 15, 108–118.
- Mittendorf, M., Papanikolaou, A., 2021. Hydrodynamic hull form optimization of fast catamarans using surrogate models. *Ship Technol. Res.* 68 (1), 14–26.
- Mohammadi, A., Sheikholeslam, F., 2023. Intelligent optimization: Literature review and state-of-the-art algorithms (1965–2022). *Eng. Appl. Artif. Intell.* 126, 106959.

- Moore, W., Mala-Jetmarova, H., Gebreslassie, M., Tabor, G., Belmont, M., Savic, D., 2016. Comparison of multiple surrogates for 3D CFD model in tidal farm optimisation. *Procedia Eng.* 154, 1132–1139.
- Moradi, M., Samwald, M., 2021. Post-hoc explanation of black-box classifiers using confident itemsets. *Expert Syst. Appl.* 165, 113941.
- Neal, R., 1998. Regression and classification using Gaussian process priors. In: Bernardo, J.M., Berger, J.O., Dawid, A.P., Smith, A.F.M. (Eds.), *Bayesian Statistics 6*. Oxford University Press.
- Nejat, A., Mirzabeygi, P., Shariat Panahi, M., 2014. Airfoil shape optimization using improved multiobjective territorial particle swarm algorithm with the objective of improving stall characteristics. *Struct. Multidiscip. Optim.* 49, 953–967.
- Nelson, M., Temple, D., Hwang, J., Young, Y., Martins, J., Collette, M., 2013. Simultaneous optimization of propeller-hull systems to minimize lifetime fuel consumption. *Appl. Ocean Res.* 43, 46–52.
- Noblesse, F., Huang, F., Yang, C., 2013. The Neumann–Michell theory of ship waves. *J. Engng. Math.* 79.
- Oneto, L., 2020. *Model Selection and Error Estimation in a Nutshell*. Springer.
- Oneto, L., Ghio, A., Ridella, S., Anguita, D., 2015. Support vector machines and strictly positive definite kernel: The regularization hyperparameter is more important than the kernel hyperparameters. In: *IEEE International Joint Conference on Neural Networks. IJCNN*.
- Orlandi, I., Oneto, L., Anguita, D., 2016. Random forests model selection. In: *European Symposium on Artificial Neural Networks, Computational Intelligence and Machine Learning*.
- Ou, M., Yan, L., Huang, W., Zhang, T., 2019. Design exploration of combinational spike and opposing jet concept in hypersonic flows based on CFD calculation and surrogate model. *Acta Astronaut.* 155, 287–301.
- Pena, B., Huang, L., 2021. A review on the turbulence modelling strategy for ship hydrodynamic simulations. *Ocean Eng.* 241, 110082.
- Peri, D., 2016. Optimal ship hull via optimal parameterisation. *Ship Technol. Res.* 63 (3), 159–170.
- Poli, R., Kennedy, J., Blackwell, T., 2007. Particle swarm optimization an overview. *Swarm Intell* 1, 33–57.
- Qu, X., Zhang, R., Liu, B., Li, H., 2017. An improved TLBO based memetic algorithm for aerodynamic shape optimization. *Eng. Appl. Artif. Intell.* 57, 1–15.
- Rasmussen, C.E., Williams, C.K.I., 2006. *Gaussian Processes in Machine Learning*. the MIT Press.
- Raul, V., Leifsson, L., 2021. Surrogate-based aerodynamic shape optimization for delaying airfoil dynamic stall using kriging regression and infill criteria. *Aerosp. Sci. Technol.* 111, 106555.
- Ray, S., 2019. A quick review of machine learning algorithms. In: *2019 International Conference on Machine Learning, Big Data, Cloud and Parallel Computing (COMITCon)*. IEEE, pp. 35–39.
- Reuther, J., Jameson, A., Farmer, J., Martinelli, L., Saunders, D., 1996. Aerodynamic shape optimization of complex aircraft configurations via an adjoint formulation. In: *34th Aerospace Sciences Meeting and Exhibit*. p. 94.
- Ruder, S., 2016. An overview of gradient descent optimization algorithms. *arXiv preprint arXiv:1609.04747*.
- Sala, A., Damalas, D., Labanchi, L., Martinsohn, J., Moro, F., Sabatella, R., Notti, E., 2022. Energy audit and carbon footprint in trawl fisheries. *Sci. Data* 9 (1), 428.
- Schulz, E., Speekenbrink, M., Krause, A., 2018. A tutorial on Gaussian process regression: Modelling, exploring, and exploiting functions. *J. Math. Psychol.* 85, 1–16.
- Sederberg, T.W., Parry, S.R., 1986. Free-form deformation of solid geometric models. *Comput. Graph. (ACM)* 20 (4), 151–160.
- Šegota, S.B., Lorencin, I., Šercer, M., Car, Z., 2021. Determining residuary resistance per unit weight of displacement with symbolic regression and gradient boosted tree algorithms. *Pomorstvo* 35 (2), 287–296.
- Serani, A., Diez, M., 2022. Parametric model embedding. <https://arxiv.org/abs/2204.05371>.
- Shalev-Shwartz, S., Ben-David, S., 2014. *Understanding Machine Learning: From Theory to Algorithms*. Cambridge University Press.
- Shamsuddin, S.M., Ahmed, M.A., Samian, Y., 2006. NURBS skinning surface for ship hull design based on new parameterization method. *Int. J. Adv. Manuf. Technol.* 28, 936–941.
- Shan, H., Jiang, L., Liu, C., 2005. Direct numerical simulation of flow separation around a NACA 0012 airfoil. *Comput. & Fluids* 34 (9), 1096–1114.
- Shao, L., Mahajan, A., Schreck, T., Lehmann, D.J., 2017. Interactive regression lens for exploring scatter plots. In: *Computer Graphics Forum*.
- Shawe-Taylor, J., Cristianini, N., 2004. *Kernel Methods for Pattern Analysis*. Cambridge University Press.
- Shi, Y., Mader, C.A., He, S., Halila, G.L.O., Martins, J.R.R.A., 2020. Natural laminar-flow airfoil optimization design using a discrete adjoint approach. *AIAA J.* 58 (11), 4702–4722.
- Shukla, K., Oommen, V., Peyvan, A., Penwarden, M., Plewacki, N., Bravo, L., Ghoshal, A., Kirby, R.M., Karniadakis, G.E., 2024. Deep neural operators as accurate surrogates for shape optimization. *Eng. Appl. Artif. Intell.* 129, 107615.
- Skinner, S., Zare-Behtash, H., 2018. State-of-the-art in aerodynamic shape optimisation methods. *Appl. Soft Comput.* 62, 933–962.
- Snyder, H., 2019. Literature review as a research methodology: An overview and guidelines. *J. Bus. Res.* 104, 333–339.
- Sobieczky, H., 1999. Parametric airfoils and wings. In: Fujii, K., Dulikravich, G.S. (Eds.), *Recent Development of Aerodynamic Design Methodologies: Inverse Design and Optimization*. Vieweg+Teubner Verlag, pp. 71–87.
- Stern, F., Wilson, R.V., Coleman, H.W., Paterson, E.G., 2001. Comprehensive approach to verification and validation of CFD simulations—Part 1: Methodology and procedures. *J. Fluids Eng.* 123 (4), 793–802.
- Strasser, G., Takagi, K., Werner, S., Hollenbach, U., Tanaka, T., Yamamoto, K., Hirota, K., 2015. A verification of the ITTC/ISO speed/power trials analysis. *J. Mar. Sci. Technol.* 20, 2–13.
- Stück, A., Rung, T., 2011. Adjoint RANS with filtered shape derivatives for hydrodynamic optimisation. *Comput. & Fluids* 47 (1), 22–32.
- Swarnkar, A., Swarnkar, A., 2020. Artificial intelligence based optimization techniques: A review. In: Kalam, A., Niazi, K.R., Soni, A., Siddiqui, S.A., Mundra, A. (Eds.), *Intelligent Computing Techniques for Smart Energy Systems*. Springer Singapore, pp. 95–103.
- Tahara, Y., Tohyama, S., Katsui, T., 2006. CFD-based multi-objective optimization method for ship design. *Internat. J. Numer. Methods Fluids* 52, 499–527.
- Tao, J., Sun, G., 2019. Application of deep learning based multi-fidelity surrogate model to robust aerodynamic design optimization. *Aerosp. Sci. Technol.* 92, 722–737.
- Tezzele, M., Fabris, L., Sidari, M., Sicchiero, M., Rozza, G., 2023. A multifidelity approach coupling parameter space reduction and nonintrusive POD with application to structural optimization of passenger ship hulls. *Internat. J. Numer. Methods Engng.* 124 (5), 1193–1210.
- Thirugnanasambandam, K., R., M., Bhattacharyya, D., Kim, J., 2022. Directed artificial bee colony algorithm with revamped search strategy to solve global numerical optimization problems. *Autom. Softw. Eng.* 29 (1).
- Upadhyay, B.D., Sonigra, S.S., Daxini, S.D., 2021. Numerical analysis perspective in structural shape optimization: A review post 2000. *Adv. Eng. Softw.* 155, 102992.
- Viana, F.A.C., 2016. A tutorial on latin hypercube design of experiments. *Qual. Reliab. Eng. Int.* 32 (5), 1975–1985.
- Vikhar, P.A., 2016. Evolutionary algorithms: A critical review and its future prospects. In: *2016 International Conference on Global Trends in Signal Processing, Information Computing and Communication. ICGTSPICC*, pp. 261–265.
- Vinuesa, R., Brunton, S., 2022. Enhancing computational fluid dynamics with machine learning.
- Vu, K., D'Ambrosio, C., Hamadi, Y., Liberti, L., 2017. Surrogate-based methods for black-box optimization. *Int. Trans. Oper. Res.* 24 (3), 393–424.
- Wainberg, M., Alipanahi, B., Frey, B.J., 2016. Are random forests truly the best classifiers? *J. Mach. Learn. Res.* 17 (1), 3837–3841.
- Walker, J.M., Coraddu, A., Oneto, L., 2024. Data-driven models for Yacht Hull resistance optimization: Exploring geometric parameters beyond the boundaries of the delft systematic Yacht Hull series. *IEEE Access* 12, 76102–76120.
- Wan, Y., Hou, Y., Xiong, Y., Dong, Z., Zhang, Y., Gong, C., 2022. Interval optimization design of a submersible surface ship form considering the uncertainty of surrogate model. *Ocean Eng.* 263, 112262.
- Wang, P., Chen, Z., Feng, Y., 2020. Many-objective optimization for a deep-sea aquaculture vessel based on an improved RBF neural network surrogate model. *J. Mar. Sci. Technol. (Jpn)*.
- Wang, Y., Joseph, J., Aniruddhan Unni, T., Yamakawa, S., Barati Farimani, A., Shimada, K., 2022b. Three-dimensional ship hull encoding and optimization via deep neural networks. *J. Mech. Des.* 144 (10), 101701.
- Wang, S., Ren, J., Fang, X., Lin, H., Xu, G., Bao, H., Huang, J., 2022a. IGA-suitable planar parameterization with patch structure simplification of closed-form polysquare. *Comput. Methods Appl. Mech. Engng.* 392.
- Wang, G.G., Shan, S., 2007. Review of metamodeling techniques in support of engineering design optimization. *Trans. ASME, J. Mech. Des.* 129 (4), 370–380.
- Wang, Y., Shimada, K., Barati Farimani, A., 2023. Airfoil GAN: encoding and synthesizing airfoils for aerodynamic shape optimization. *J. Comput. Des. Eng.* 10 (4), 1350–1362.
- Wang, Q., Wang, J., Chen, J., Luo, S., Sun, J., 2015. Aerodynamic shape optimized design for wind turbine blade using new airfoil series. *J. Mech. Sci. Technol.* 29, 2871–2882.
- Wolpert, D.H., 2002. The supervised learning no-free-lunch theorems. *Soft Comput. Ind.: Recent Appl.* 25–42.
- Yan, X., Zhu, J., Kuang, M., Wang, X., 2019. Aerodynamic shape optimization using a novel optimizer based on machine learning techniques. *Aerosp. Sci. Technol.* 86, 826–835.
- Yilmaz, N., 2022. Comparative energy and environmental assessment of battery technologies and alternative fuels in sustainable aviation. *Int. J. Green Energy* 1–10.
- Zhang, T., Huang, W., Wang, Z., Yan, L., 2016. A study of airfoil parameterization, modeling, and optimization based on the computational fluid dynamics method. *J. Zhejiang Univ.-Sci. A (Appl. Phys. Eng.)* 17 (8), 632–645.
- Zhang, S., Tezdogan, T., Zhang, B., Lin, L., 2021b. Research on the hull form optimization using the surrogate models. *Eng. Appl. Comput. Fluid Mech.* 15, 747–761.

Zhang, S., Tezdogan, T., Zhang, B., Xu, L., Lai, Y., Zhang, S., 2017. Hull form optimisation in waves based on CFD technique. *Ships Offshore Struct.* 5302 (August).

Zhang, D., Wang, Z., Ling, H., Zhu, X., 2021a. Kriging-based shape optimization framework for blended-wing-body underwater glider with NURBS-based parametrization. *Ocean Eng.* 219, 108212.

Zhang, B.J., Zhang, Z.X., 2015. Research on theoretical optimization and experimental verification of minimum resistance hull form based on rankine source method. *Int. J. Nav. Architect. Ocean Eng.* 7 (5), 785–794.